BOEING SCIENTIFIC RESEARCH LABORATORIES DOCUMENT D1-82-0871

BOEING

SCIENTIFIC RESEARCH LABORATORIES

Response of an Acoustically Loaded Panel Excited by Supersonically Convected Turbulence

L. Maestrello

T. L. J. Linden

SCIENCES LABORATORY MAY 1970

51

D1-82-0971

RESPONSE OF AN ACOUSTICALLY LOADED PANEL EXCITED BY SUPERSONICALLY CONVECTED TURBULENCE

L. Maestrello

T. L. J. Linden

This project which is a continuation of BSRL Document D1-82-0719 was jointly supported by The Boeing Company and NASA Langley. Part of this study was performed while one of the authors (Maestrello) was visiting at BSRL.

Contents

SUMMARY

Measurements have been made of the wall pressure fluctuation and the response of the panel structure. The plate is excited by a boundary layer (M=3.03) and shock inpingement (° angle) the flow downstream of the shock is separated. The wall pressure fluctuations and panel displacement are notably greater than the case without the shock present.

The response of a plate clamped in a baffle is determined. The plate is coupled acoustically to a uniformly moving fluid. The boundary-layer exciting the plate does not interact with the acoustic field and is furthermore taken to be spatially uncorrelated. Finally, the radiation is determined over the solid angle of the Mach cone. The response is derived using finite Fourier transforms and then solving the resulting algebraic equation by expressing the solution expanded in a complete set of functions, a process which leads to an infinite set of linear equations. The right-hand side of this system of equations is a stochastic variable so that performing an ensemble average the resulting equation is solved for the covariance matrix which is subsequently diagonalized to yield the power spectral density in the statistically independent states (degrees of freedom).

Description of the actual computations will be reported at a later date.

1. INTRODUCTION

A large aircraft in supersonic flight undergoes large variations in flow field over its surface. This paper is concerned with studying the response of a structure excited by convected turbulence at nearly zero pressure gradient and by shock-boundary layer interaction, with the inclusion of the coupling due to the acoustic field on each side of a panel. Shock waves on thin-walled structures can impose severe loading problems, the most common of which is the self-induced oscillation which is generated by an oscillating shock. The shock wave can easily couple with the forcing frequency present in the environment, including panel resonances.

From interior noise point of view, the upper region of the airplane fuselage is considered the principal noise radiator. The aerodynamics in this region are known from the Prandtl-Mayer relation, and further downstream by shock-boundary interaction. In addition, the fuselage skin experiences traveling shock waves which run up and down the skin during the acceleration period, which might last twenty minutes for a Mach 3 airplane.

In supersonic flight, the vibration of the surface is influenced by the back pressure resulting from the radiation of sound on both sides of the surface, so that, the surface motion and radiation are coupled phenomena. The interior noise level is determined by skin panel vibrations. For radiation below the critical frequency, the major source of sound arises from the interaction of the bending wave with the discontinuity of the boundary. Above the critical frequency, the action of discontinuities like tear stoppers, etc., have little effect on altering sound pressure level, since the sound radiated by the panel is in the form of Mach wave radiation.

The experiment described in this paper indicates that some simplifications in the model can be made, viz. (1) that there is no significant interaction between the plate and the aerodynamic forces on the plate; and (2) that the panel displacement is small in comparison to its thickness so that thin

plate theory may be used. The plate, is however, acoustically coupled to the external flow field and the internal cavity.

Lyamshev (1968) has solved a similar problem for a complex structure. Dowell (1969) computed the transient, non-linear response of a simply supported plate coupled to an external flow field and a cavity. Dżygadlo (1967) presented a linear analysis allowing mutual interaction between the plate and the external flow. Fahy and Pretlove (1967) have computed a first order approximation to the acoustic coupling of a flexible duct wall to the flow field through the duct. Maidanek (1966) considers an infinite, orthotropic plate coupled acoustically to an external flow field. Numerous other investigations have been reported on acoustically coupled structures with varying degrees of approximation, Irgens and Brand (1968), White and Cottis (1968), Strawderman (1967), Creighton (1970), Ffowcs-Williams (1966), Crighton and Ffowcs-Williams (1969), Dolgova (1969), Feit (1966), Lapin (1967), Pal'tov and Pupyrev (1967).

2. MEASUREMENTS

a) The Experimental Arrangement

The flow investigated was the sidewall boundary layer of the Jet Propulsion Laboratory 20-inch supersonic wind tunnel; the shock was induced by a 30° wedge mounted outside the boundary layer, off-center and on the same side that the measurements were made. This was done to offset the position of the reflected shock from the opposite wall. The position of the shock was determined by observing the displacement of a line of tufts, and by a static pressure survey. For zero pressure gradient, detail of flow field and panel response has been previously reported by Maestrello (1968).

The experiment was arranged to perform three basic measurements: mean velocity profile ahead of the shock with static pressure distribution across the shock, wall pressure fluctuations and measurement of displacement response of a simple panel structure. The titanium* test panel measured 12 x 6 x .062 inches and was brazed on all four sides of a 3/4 inch x 3/4 inch titanium frame. The brazing was intended to simulate the clamped edge condition. The panel formed most of one wall of a rigid cavity measuring 14 x 8 x 6.6 inches. The other surface of the panel was exposed to the flow field. The pressure differential across the panel was variable. The experiment was conducted at two pressure differentials, viz, 0.06 and 14 psi; the latter corresponds to the actual differential between wind tunnel pressure and local ambient.

The side wall of the tunnel was modified to accommodate two identical, rigid, steel plates, which supported the necessary instrumentation. One plate contained an array of holes in which pressure transducers were mounted. The pressure transducers were mounted on the center-line of the tunnel in the streamwise direction at the same locations where the

---

*TI-6AL-4V Titanium alloy containing 6% aluminum, 4% vanadium, 90% titanium

mean static pressure measurements were made. Two types of pressure transducers were used; one, the conventional lead-zirconate titanate type made by Atlantic Research, the other a capacitance type made by Photocon Corporation with sensitive diameters of 0.06 inch and 0.09 inch respectively. Correction due to finite size transducers was made adopting the Corcos (1963) approach. The panel displacement was measured with Photocon capacitance, displacement transducers mounted on brackets which could slide along a bar and could be set precisely by means of a screw mechanism.

The output of both pressure transducers and displacement transducer were recorded on Ampex FR-1800H 14-channel tape, recorded in the FM mode. Four channels were used for simultaneously recording data for correlation measurements. The maximum dynamic range was obtained by splitting each data channel into two tape tracks through phase matched filters to separate the lower and higher frequencies.

b) The Wall Pressure Field

Measurements indicated that the flow field in front of the shock closely approximated the properties of equilibrium of an adiabatic flat-plate boundary layer (Maestrello 1968). The flow in front of the shock has the following characteristics: Mach number $M_e = 3.03$, free stream velocity $U_e = 2,100$ ft/sec, total temperature $T_t = 567°$ R, boundary layer thickness $\delta = 1.37$ inch. boundary layer displacement thickness $\delta^* = 0.445$ inch, momentum thickness $= 0.083$ inch, Reynolds number $R = U_e \delta / U = 4.87 \times 10^5$, skin friction coefficient $C_f = 1.27 \times 10^{-3}$, and $\bar{C}_f \bar{R}_\theta = 39.8$ Coles parameter (Coles 1964).

The pressure ratio across the shock is a well defined function of Mach number, for a 15° half-cone angle, the pressure ratio is approximately 8.5. Experimental results show, however, that this ratio is considerably smaller ($\Delta p = 2.3$). It is postulated that interaction with an expansion

wave originating at the base of the wedge is responsible for lowering the pressure differential and producing an effective decay downstream, Figure 1. In the present case, the wedge angle induces a shock in the boundary layer large enough to cause a separation: farther downstream, the flow becomes reattached and goes back to the flat plate condition. This transition takes place within a few boundary layer thicknesses.

Downstream of the shock, the ratio of the mean pressure distribution p_{sd}/p_s and the ratio of the rms pressure fluctuation p'_{sd}/p'_s vary with a consistent relationship and both reach a maximum at $x/\delta \simeq 2.3$, where subscripts s and sd, mean upstream and downstream of the shock, respectively, Figure 1. Beyond $x/\delta \simeq 6$ the effect of the shock on the static pressure vanishes. Kistler (1963) indicates a similar behavior between mean and fluctuating pressure in the separated region ahead of a forward-facing step at the same Mach number and upstream Reynolds number. The differences in the flow geometry only alter the magnitude of the pressure, in that the ratio of the mean pressure to the fluctuating pressure $p_{sd}/p'_{sd} \simeq 14$ in the present experiment while Kistler found that $p_{sd}/p'_{sd} \simeq 32$.

The normalized power spectral density measured upstream and downstream of the shock are shown in Figure 2. The spectra are normalized by requiring $\int_0^\infty \pi(\omega)\, d = 1$ in order to demonstrate the deviation from the zero pressure gradient ease. For the spectra just downstream of the shock more energy is concentrated in a narrow low frequency band while further downstream at $x/\delta \simeq 4$, the energy is distributed over a much broader bandwidth and approaches the shape and level of the spectrum taken upstream of the shock. The normalized power spectral density found upstream of the shock corresponds to the zero pressure gradient, and peaks at $\omega\delta/U_e \simeq 2$ while downstream the spectral density is modified in the region below the peak. It is significant that by altering the local flow

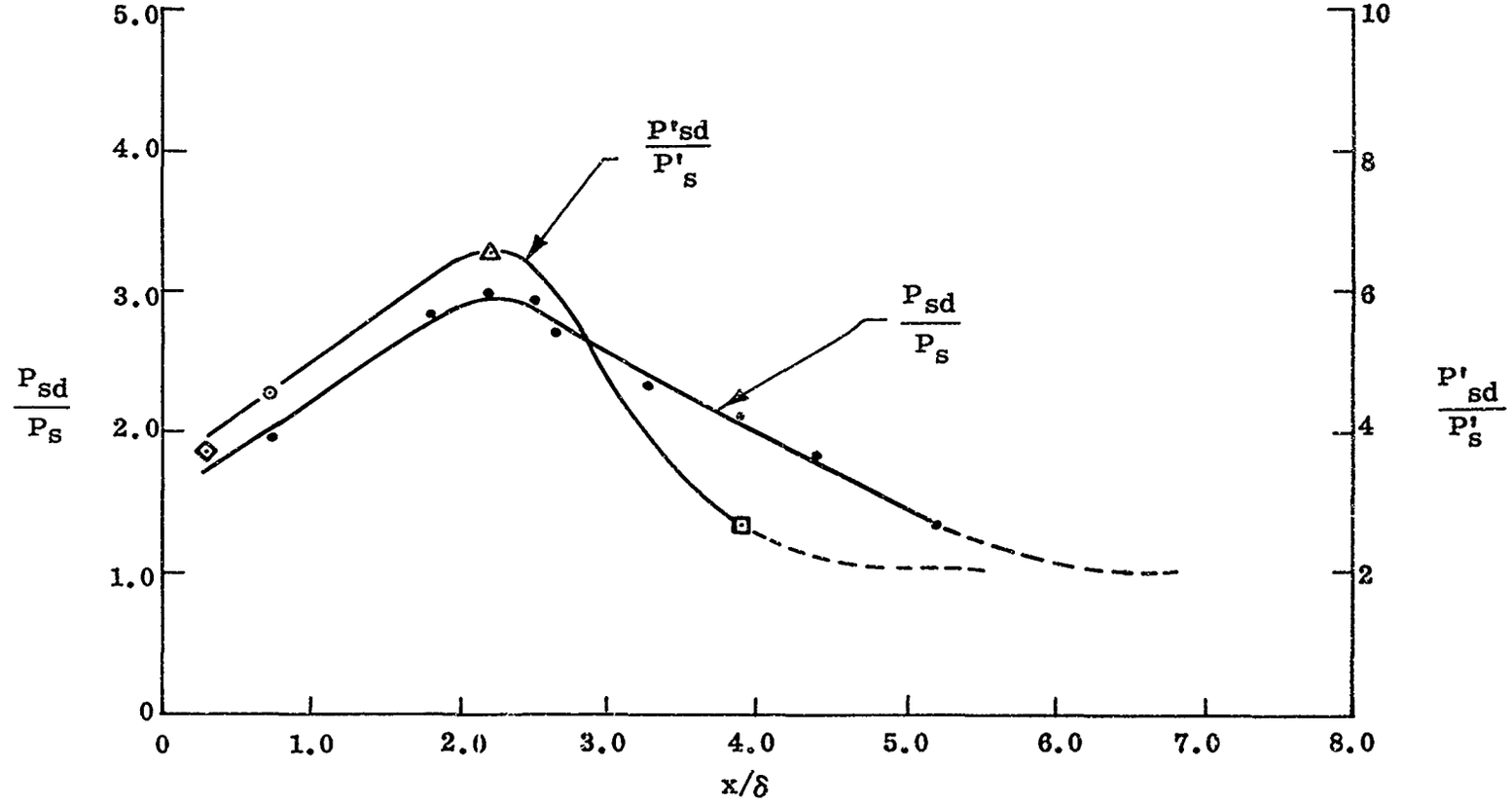

Figure 1. Static Pressure Fluctuations and Mean Pressure Distribution Downstream of the Shock.

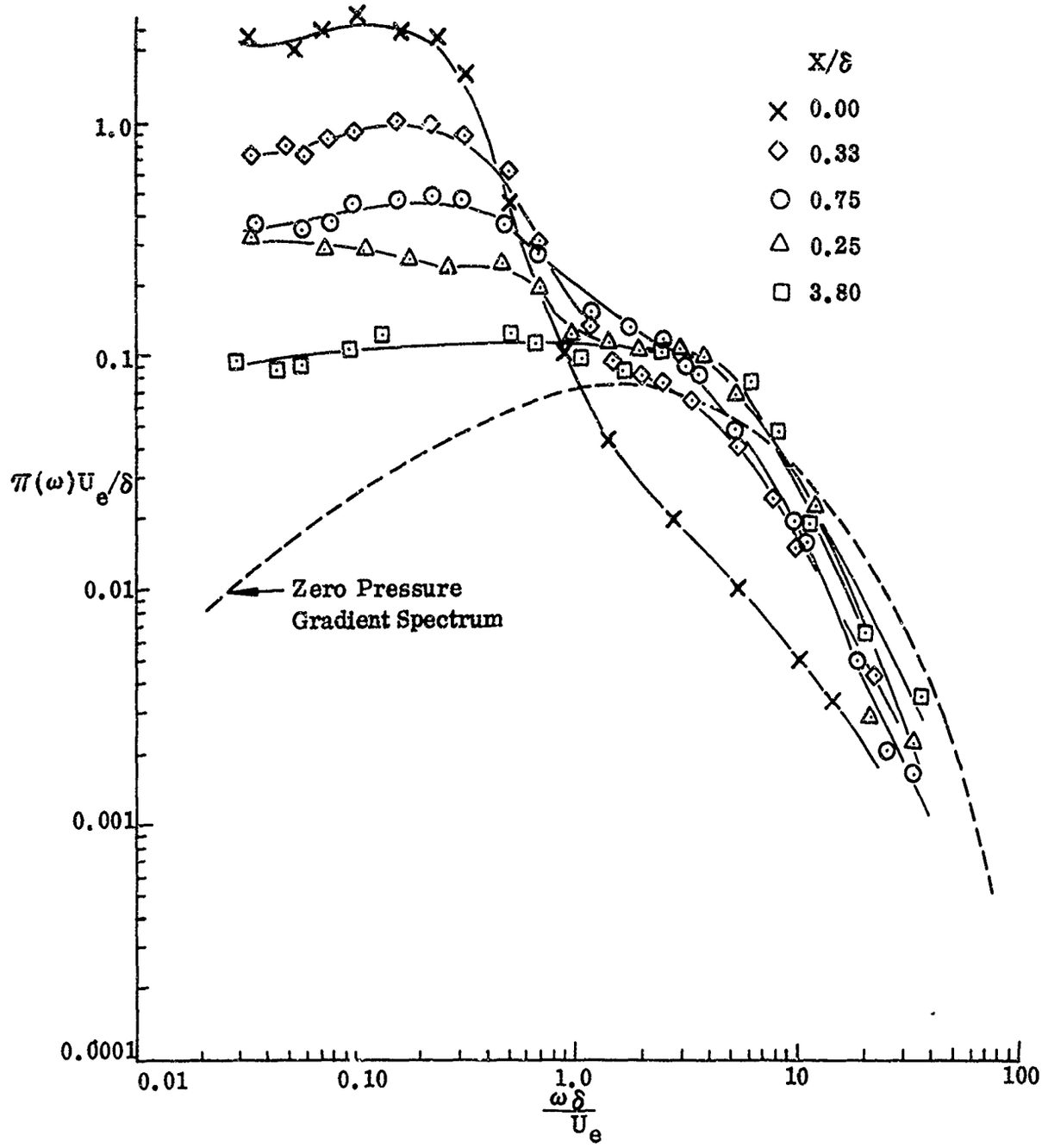

Figure 2. Power Spectral Density of the Wall Pressure Fluctuations

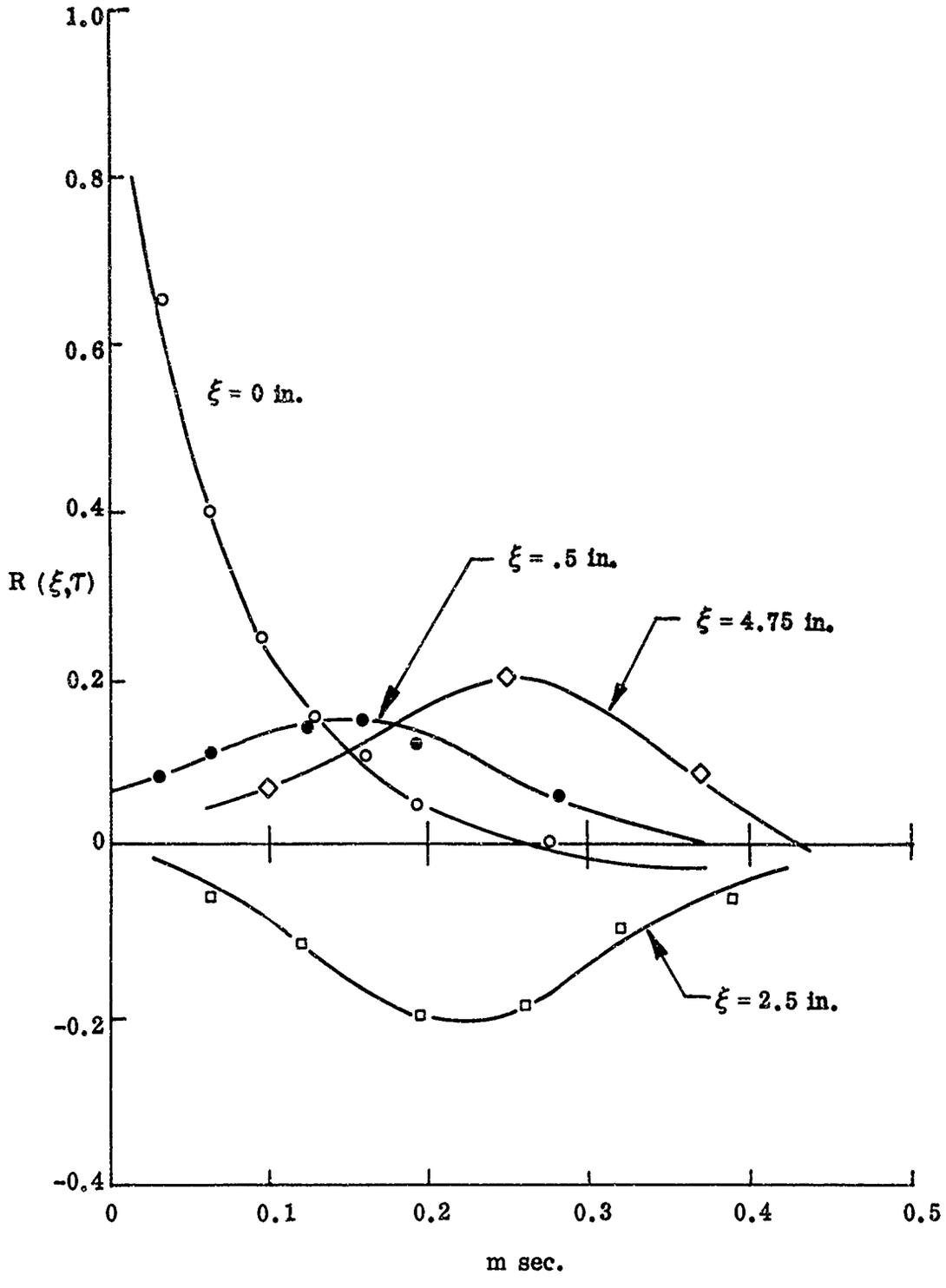

Figure 3. Longitudinal Cross-Correlation of The Wall Pressure

conditions, only the low frequency ends of the spectra are appreciably affected. It is noticed that the pressure fluctuation measurements at $x/\delta \simeq 0$ where the shock impinges show a noticeable deviation from the general pattern in the higher frequencies. This is attributed to an intermittant signal superimposed on the regular pressure signal as seen on the oscilloscope. It is possibly due to the characteristic fanning of the shock as it goes through the boundary layer.

Measurements of the cross-correlation are shown in Figure 3. The cross-correlation characteristics are a function of position downstream of the shock. The cross-correlation between positions $x/\delta = 0.33$ and $x/\delta = 3.80$, the farthest apart, has characteristics similar to those found at zero pressure gradient boundary layer in that the ratio between the convection velocity and the freestream velocity $U_c/U_e = 0.72$ and that the correlation between those two points is still significant. The cross correlation of the shortest distance between $x/\delta = 0.33$ and $x/\delta = 0.75$, shows that the convection velocity is very low $U_c/U_e = 0.13$ and the correlation is very weak. The correlation between $x/\delta = 0.33$ and $x/\delta = 2.25$, where $x/\delta = 2.25$ corresponds to the maximum static pressure ratio is negative. The shock induces the boundary layer to separate and the recirculation within the separation region permits the sign of the pressure to change. Kistler argued that the fluctuating pressure in the separated region arises from the combined action of the turbulent shear layer and the recirculating flow. The picture, however, is not yet clear enough to develop a model for time dependent loading, since the geometry of the separated region is the primary variable in estimating the pressure amplitude and resulting phase.

No measurement of the lateral cross-correlation was made during the test; however, for the purpose of computing the response of the panel, it is assumed that the pressure decays similarly to that in the case of zero pressure gradient $e^{-|\eta|/\alpha_2}$ where $\alpha_2 = 0.26$ and η is the spatial separation (Maestrello 1968).

This choice overestimates the lateral cross-correlation, since the flow field is far from being homogeneous. However, the overestimation may not be exceeded by a factor of 2.

c) The Panel Response Field

Measurements were made of the power spectral density and cross-correlation of the displacement. Typical results are shown in Figures 4, and 5 for a pressure differential of 14 psi. The static deflection of the panel was 0.06 inches at the center, and the dynamic deflection was small in comparison with its thickness.

The displacement spectral density at the center of the panel show pronounced spikes, the lowest frequency of which corresponds to the lowest mode of the panel. The accuracy beyond a frequency of 3100 Hz was poor due to the spatial resolution of the capacitance transducer, and therefore the spectrum beyond 3100 Hz was ignored.

Space-time correlation measurements were made along the panel centerline from $x = x' = 3$ in. $y = y' = 3$ in. at one-inch intervals up to a maximum separation of 6 in. The correlogram indicates a convected feature with a phase velocity $\pm U_{cp} = 770$ ft/sec. This convection velocity corresponds to that found in the previous experiment using the same arrangements, except that no shock was present (Maestrello 1968).

In comparing the results of the present and previous experiments, it is concluded that the sign change of the convection velocity is attributed to the presence of the shock. Furthermore, the cross-correlation of the wall pressure also reflects a phase change for a separation of 2.5 inches, which is in the same location as the phase change which occurs for the displacement correlation in Figure 5.

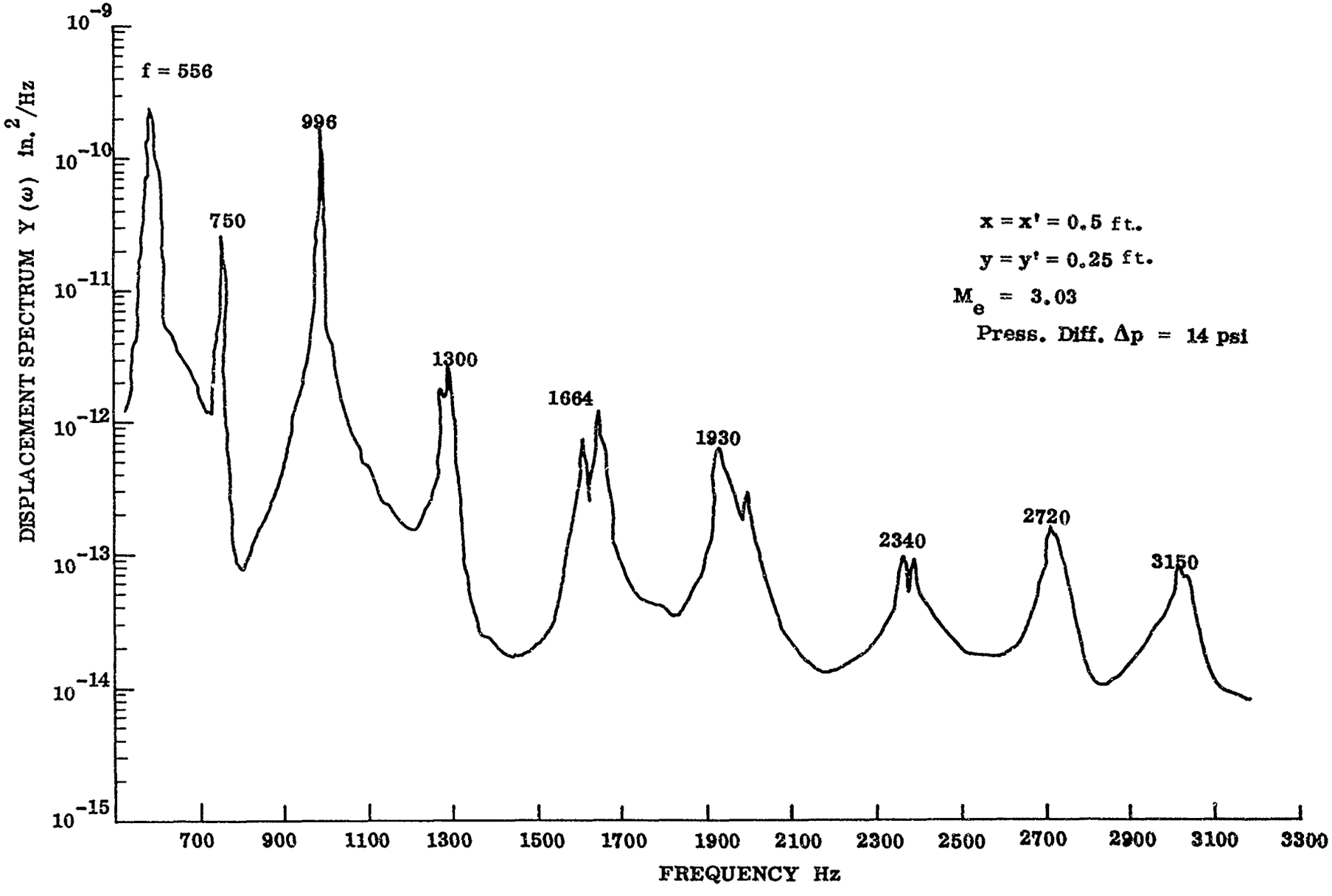

Figure 4. Displacement Spectral Density

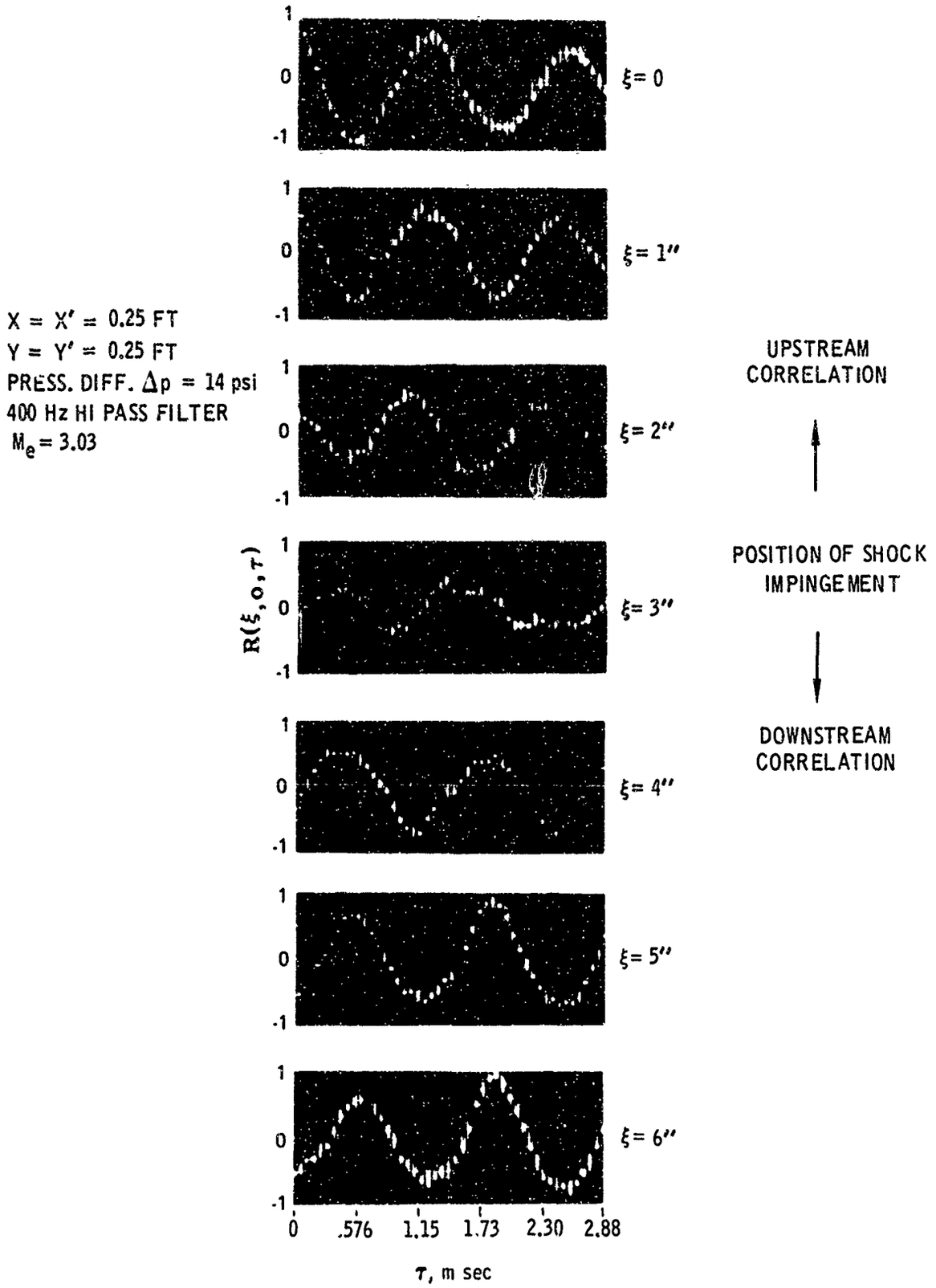

Figure 5. Broad Band Space Time Correlation of the Panel Displacement Along the Center from x = x' = 0.25 Ft. y = y' = 0.25 Ft.

3. ANALYSIS OF ACOUSTICALLY COUPLED PANELS

a. Two-dimensional Finite Panel

The vibration of the panel is induced by an arbitrary, external pressure field F. It is assumed that the panel motion does not interact with the turbulent boundary layer, i.e., the forcing field is not altered by the plate motion. However, the panel is acoustically coupled to the fluid on both sides of the panel.

The equation of motion for an harmonic component of the displacement, W, of a thin panel with a force, F, and a pressure differential, $p_2 - p_1 + \delta p$ acting upon it, obeys the equation

$$B \Delta^2 W - \rho_p \omega^2 W = F + p_2 - p_1 + \delta p \qquad (1)$$

where the bending stiffness, B, may include hysteretic damping, and where ρ_p is the mass per unit area of the panel, ω is the angular frequency, p_2 is the acoustic pressure on the streamside of the panel, p_1 is the acoustic pressure below the panel and δ_p is the static pressure differential.

The perturbation pressures, p_1 and p_2, are related to the velocity potentials, which satisfy time-independent wave equations in the appropriate regions. In solving these equations one uses a boundary condition which relates the potentials to the panel displacement. These relationships may be made more obvious through the use of Green's theorem. Thus, it is required to solve a system of three coupled partial differential equations, the first of which is not separable for the clamped edge boundary condition.

p_1 and p_2 may be found directly as function of W. Thus, consider first the cavity. The acoustic velocity potential, φ, satisfies the Helmholtz equation

$$\Delta \varphi + k^2 \varphi = 0 \qquad (2)$$

with boundary condition $\frac{\partial \varphi}{\partial n} = 0$ on all walls except on the plate where $\frac{\partial \varphi}{\partial n} = -i\omega W$.

The Greens function, g, for a cavity with hard walls satisfies the equation

$$\Delta\ g\ (\vec{r} \mid \vec{r}') + k_c^2 g\ (\vec{r} \mid \vec{r}') = -4\pi \delta (\vec{r} - \vec{r}') \tag{3}$$

and is given by Morse and Feshbach, Vol. II (1953)

$$g\ (r/r') = -\frac{4\pi}{a_c b_c} \sum_{m=0} \sum_{n=0} \varepsilon_m \varepsilon_n \frac{\cos \frac{m\pi x}{a_c} \cos \frac{m\pi x}{a_c} \cos \frac{n\pi y}{b_c} \cos \frac{n\pi y'}{b_c}}{k_{mn} \sin (k_{mn} d)} X \tag{4}$$

$$\begin{cases} \cos\ k_{mn} z \cos\ k_{mn} (z' + d) & z > z' \\ \cos\ k_{mn} z' \cos\ k_{mn} (z + d) & z < z' \end{cases}$$

where $k_{mn}^2 = k_c^2 - \left(\frac{m\pi}{a_c}\right)^2 - \left(\frac{n\pi}{b_c}\right)^2$

and $k_c = \omega / c_c$ where c_c is the speed of sound in the cavity of dimensions a_c, b_c, d.

By applying Green's theorem, the integral equation for φ is obtained,

$$\varphi (\vec{r}) = \frac{1}{4\pi} \iint_{\text{plate}} g\ (\vec{r}/\vec{r}_s') \frac{\partial \varphi (\vec{r}_s')}{\partial n'} d\vec{r}_s' \tag{5a}$$

Now using the boundary conditions, this becomes

$$\varphi (\vec{r}) = -\frac{i\omega}{4\pi} \iint_{\text{plate}} g\ (\vec{r}\ \vec{r}_s')\ W\ (\vec{r}_s')\ d\vec{r}_s' \tag{5b}$$

The pressure p_1 is related to φ by

$$p_1 = -i\omega\rho_c\varphi$$

where ρ_c is mass density of the fluid in the cavity.

To compute p_2, it will be more convenient to operate with the differential equation. Let the acoustic velocity potential in the flow field be denoted by ψ. By applying the Fourier transform on the (x, y) coordinates, one gets the ordinary differential equation

$$\frac{d^2\psi(\alpha, \beta, z)}{dz^2} + \zeta^2 \hat{\psi}(\alpha, \beta, z) = 0 \qquad (6)$$

where

$$\zeta^2 = k^2 + (M^2 - 1)\alpha^2 - 2kM\alpha - \beta^2$$

$$\psi(x, y, z) = \int_{-\infty}^{\infty}\int_{-\infty}^{\infty} d\alpha d\beta e^{i(\alpha x + \beta y)} \hat{\psi}(\alpha, \beta, z)$$

$k = \omega/c$, M is the flow Mach number and c the speed of sound in the region above the plate. Only the positive exponential solution to equation (6) is chosen, since it is the solution representing outgoing waves. Thus,

$$\hat{\psi}(\alpha, \beta, z) = A(\alpha, \beta) e^{i\zeta z} \qquad (7a)$$

The boundary condition, arising from the continuity of normal displacement

is

$$\frac{d\hat{\psi}(\alpha,\beta,z)}{dz} = -ic\,\hat{LW}$$

where the differential operator

$$L = k + i\,M\frac{\partial}{\partial x}$$

Thus,

$$\hat{\psi}(\alpha,\beta,z) = -c\frac{\hat{LW}}{\zeta}e^{i\zeta z} \tag{7b}$$

Now, since

$$\hat{LW} = \int_0^a\int_0^b dx'dy'\,e^{-i(\alpha x' + \beta y')}L\,W(x',y')$$

then

$$\psi(x,y,z) = -\frac{c}{4\pi^2}\int_0^a\int_0^b dx'dy'\,G(x,y,z\,|\,x',y',o)\,L\,W(x',y') \tag{8}$$

where

$$G(\vec{r}\,|\,\vec{r}') = \int_{-\infty}^{\infty}\int_{-\infty}^{\infty} d\alpha d\beta\,\frac{e^{i[\alpha(x-x') + \beta(y-y') + \zeta(z-z')}}{\zeta} \tag{9}$$

which is found in Appendix A to be for supersonic flow,

$$G(\vec{r}\,|\,\vec{r}') = \begin{cases} \dfrac{2\pi i}{\sqrt{M^2-1}}\;\dfrac{e^{i\kappa(Mu + \sqrt{u^2 - R^2}}}{\sqrt{u^2 - R^2}} \\ o \qquad \text{outside the Mach cone} \end{cases}$$

and for subsonic flow,

$$G(\vec{r}\,|\,\vec{r}') = \frac{2\pi i}{\sqrt{1-M^2}} \frac{e^{i\kappa(Mu+\sqrt{u^2+R^2})}}{\sqrt{u^2+R^2}} \tag{10}$$

except in this case, $\kappa = \frac{k}{\sqrt{1-M^2}}$ and $u = \frac{x-x'}{\sqrt{1-M^2}}$

If $\hat{LW}$ had been evaluated as

$$(k - \alpha M)\,\hat{W}$$

then equation (8) would read

$$\psi(x, y, z) = -\frac{c}{4\pi^2}\int_0^a\int_0^b dx'dy'\, W(x', y')\, L^*G(x, y, z\,|\,x', y, z') \tag{11}$$

This equation is formally correct if L^*G is interpreted as a distribution, which is to say that one partially integrates to obtain equation (8).

Now using equation (8)

$$p_2(x, y, z) = -i\rho_o c\, L\psi(x, y, z)$$

$$= \frac{i\rho_o c^2}{4\pi^2}\int_0^a\int_0^b dx'dy'\, G(x, y, z\,|\,x', y', o)\,|L|^2\, W(x', y') \tag{12}$$

where ρ_o is the density of the fluid above the plate, and where partial integration has been utilized. Had equation (11) been used instead, equation (12) would read

$$p_2(x, y, z) = \frac{i\rho_o c^2}{4\pi^2}\int_0^a\int_0^b dx'dy'\, W(x, y)\,|L|^2\, G(x, y, z\,|\,x', y', o) \tag{13}$$

which is reducible to equation (12) by partial integration. Thus, supersonic flow does not present any especial difficulty aside from the fact that G is singular all along the Mach cone, and this is an integrable singularity.

Inserting the expressions for p_2 and p_1 into equation (1) results in a single partial integro-differential equation to solve, viz.,

$$B\Delta^2 W - \rho_p \omega^2 W = F + \delta_p + \frac{i\rho_o c^2}{4\pi^2} \int_0^a \int_0^b G(x, y, | x', y') |L|^2 W(x', y') dx' dy'$$

$$+ \frac{\omega^2 \rho_c}{4\pi} \iint_{\text{plate}} g(x_c, y_c | x_c', y_c') W(x, y) dx dy \qquad (14)$$

where the subscript c refers to the cavity, thus

$$x_c = x + \frac{a_c - a}{2}$$

$$y_c = y + \frac{b_c - b}{2}$$

Equation (14) presents a formidable computational problem. The Green's function g is known as an infinite series which is slow to converge (1/n) thus compounding the difficulty by an increasing number of necessary operations to maintain a given accuracy.

An alternative to solving equation (14) is to convert it to an integral equation for its Fourier amplitudes and to solve the resulting equation. The advantage is that this equation is simpler (though it is a singular integral equation). The following notation shall be employed:

$$\hat{f}(\vec{K}) = \frac{1}{2\pi} \int_{\text{supp}\ \{f\}} d\vec{r}\ e^{-i\vec{K}\cdot\vec{r}} f(\vec{r})$$

$$f(\vec{r}) = \frac{1}{2\pi} \int_{\vec{K}\text{-space}} d\vec{K}\ e^{i\vec{K}\cdot\vec{r}} \hat{f}(\vec{k})$$

The result of applying the Fourier transform to equation (1) is

$$B\hat{\Delta^2 W} - \rho_p \omega^2 \hat{W} = \hat{f} + \hat{p}_2 - \hat{p}_1 \tag{15}$$

where

$$f = F + \delta_p$$

The first term in (15) may be evaluated using Green's theorem; thus,

$$\hat{\Delta^2 W} = K^4 \hat{W} + \oint d\vec{r}_s \frac{\partial}{\partial n} \left[e^{-i\vec{K}\cdot\vec{r}} (\Delta W + K^2 W) \right] \tag{16a}$$

Now, for a plate clamped on its edge to a rigid, plane support, the following boundary conditions hold,

$$\left.\begin{aligned} W &= \partial_n W = 0 \\ \frac{\partial^2 W}{\partial s^2} &= \frac{\partial^3 W}{\partial n\, \partial s^2} \end{aligned}\right\} \text{ on edge}$$

Where s is in the direction of the edge, i.e., the tangent, Thus,

$$\hat{\Delta^2 W} = K^4 \hat{W} + \Lambda \left[W \right] \tag{16b}$$

where

$$\Lambda\left[W\right] = \oint d\vec{r}_s \left(\frac{\partial^3 W}{\partial n^3} - i (\vec{K} \cdot \vec{n}) \frac{\partial^2 W}{\partial n^2} \right) e^{-i \vec{K} \cdot \vec{r}_s}$$

If more general boundary conditions are to be considered (e.g. elastic foundation) the above expression must be replaced by the right side of 16a. From the equation (7b) and the equation prior to equation (12) it is found that

$$\hat{p}_2 = \frac{i \rho_o c^2 (k - \alpha M)^2}{\zeta} \hat{W}(\vec{K}) \tag{17}$$

From equation (5b) it is found that

$$\hat{p}_1 = -\frac{\omega^2 \rho_p}{4\pi} \int_{\text{plate}} d\vec{r}_s \, g(\vec{K} | \vec{r}_s) \, W(\vec{r}_s)$$

$$= -\Omega\left[W\right]$$

where

$$g(\vec{k} | \vec{r}') = \frac{1}{2\pi} \int_{\text{plate}} d\vec{r} \, e^{-i \vec{k} \cdot \vec{r}} \, g(\vec{r} | \vec{r}') \tag{18}$$

Substituting these results into equation (15) gives

$$\Upsilon(\vec{K}) \hat{W}(\vec{k}) + B\Lambda\left[W\right] - \Omega\left[W\right] = \hat{f}(\vec{K}) \tag{19}$$

where

$$\Upsilon(K) = K^4 - \frac{\rho_s \omega^2}{B} - \frac{i \rho_o c^2 (k^2 - \alpha^2 M^2)}{B \zeta} \tag{19a}$$

Let ψ_n denote the finite Fourier transform of a beam eigen function, φ_n. It follows from the Fourier representation that the ψ_n form an orthogonal set on the infinite interval. Thus, expanding $\hat{W}$ as

$$\hat{W}(\vec{K}) = \sum_{m,n} W_{mn} \psi_m(\alpha a) \psi_n(\beta b) \tag{20}$$

or alternatively, W as

$$W(\vec{r}) = \sum_{m,n} W_{mn} \varphi_m\left(\frac{x}{a}\right) \varphi_n\left(\frac{y}{b}\right) \tag{21}$$

and introducing these expressions into (19) and subsequently utilizing the orthogonality, gives

$$W_{mn} + \sum_{r,s} \Gamma_{mnrs} W_{rs} = \Phi_{mn} \tag{22}$$

where Φ_{mn} are the projections of

$$\Phi(\vec{k}) = \frac{\hat{f}(\vec{K})}{\Upsilon(\vec{K})}$$

$$= \sum_{m,n} \Phi_{mn} \psi_m(\alpha a) \psi_n(\beta b)$$

and

$$\Gamma_{mnrs} = \int_{-\infty}^{\infty}\int_{-\infty}^{\infty} d\vec{K} \frac{\psi_m^*(\alpha a)\psi_n^*(\beta b)}{\Upsilon(\vec{K})} \left(B\Lambda\left[\varphi_r\left(\frac{x}{a}\right)\varphi_s\left(\frac{y}{b}\right)\right] - \right.$$

$$\left. - \Omega\left[\varphi_r\left(\frac{x}{a}\right)\varphi_s\left(\frac{y}{b}\right)\right]\right)$$

(See Appendices B, C and D)

The computation of the integral Γ_{mnrs} may be simplified by deforming the contour on the α- plane. Due to the manner in which the Fourier transform was chosen, the integrand, except the term $\Upsilon(\vec{k})$, is single-valued and analytic in the lower half-plane. The contour will, thus, be deformed in this half-plane. This deformation is determined by the analytic properties of the function $\Upsilon(\vec{k})$, equation 19a.

$$\Upsilon(\alpha,\beta) = (\alpha^2+\beta^2)^2 - \frac{\rho_p\omega^2}{B} \frac{i\frac{\rho_o\omega^2}{B}\left(1-\frac{\alpha^2 M^2}{k^2}\right)}{\sqrt{k^2+(M^2-1)\alpha^2 - 2kM\alpha - \beta^2}}$$

This function is two-sheeted with square-root type branch points at

$$\frac{kM \pm \sqrt{k^2+(M^2-1)\beta^2}}{M^2-1}$$

The sheet associated with the positive value of the squre root will be termed the physical sheet, since it corresponds to outgoing radiation.

The function has ten zeros on the two sheets, four zeros on each sheet with the same values, corresponding to resonances of the plate and the other two zeros are located near the branch points on one of the two sheets, independent of each other.

It is convenient to make the following substitutions

$$\mu = \frac{\rho_o}{\rho_p} \quad \text{and} \quad \gamma^4 = \frac{\rho_p\omega^2}{B}$$

The equation (19a) may be written

$$\Upsilon(\alpha,\beta) = (\alpha^2+\beta^2)^2 - \gamma^4 - \frac{i\mu\gamma^4\left(1-\left(\frac{\alpha^2 M^2}{k^2}\right)\right)}{\sqrt{k^2+(m^2-1)\alpha^2 - 2kM\alpha - \beta^2}}$$

In the present case μ is a small number ($\approx .0015$) so that approximate values of the zeros may be found, expressed as a power series in μ. To the second order these zeros are

$$\alpha_s^{\pm} = A_s^{\pm} - \frac{\mu^2}{2} \frac{\left[1 - \left(\frac{A_s^{\pm 2} M^2}{k^2}\right)^2\right] \gamma^8}{\sqrt{(k^2 + (M^2-1)\beta^2)(A_s^{\pm 4} + 2 A_s^{\pm 2} \beta^2 + \beta^4 - \gamma^4)^2}}$$

where

$$A_s^{\pm} = \frac{k M \pm \sqrt{k^2 + (M^2 - 1)\beta^2}}{M^2 - 1}$$

$$\alpha_{(\pm)_1(\pm)_2} = A_{(\pm)_1(\pm)_2} + \mu \frac{i \gamma^4 \left[1 - \left(\frac{M A_{(\pm)_1(\pm)_2}}{k}\right)^2\right]}{4 A_{(\pm)_1(\pm)_2} (\beta^2 + A^2_{(\pm)_1(\pm)_2}) \left[k^2 + (M^2-1) A^2_{(\pm)_1(\pm)_2} - 2 k M A_{(\pm)_1(\pm)_2} \beta^2\right]^{1/2}}$$

where

$$A_{(\pm)_1(\pm)_2} = (\pm)_1 \sqrt{-\beta^2 - (\pm)_2 \gamma^2}$$

The last four zeros exist on both sheets. The location of the first two zeros may be distinguished into three possibilities: when $\gamma < A_s^-$ then α_s^- and α_s^+ are respectively on the unphysical and physical sheets; as γ is increased such that $A_s^- < \gamma < A_s^+$, then α_s^- moves off the unphysical sheet and crosses over to the physical sheet and α_s^+ remains unchanged; as γ is further increased such that $A_s^+ < \gamma$ then α_s^+ crosses over to the unphysical sheet and α_s^- remains unchanged. A typical configuration for the poles and branch points is shown in Figure 6.

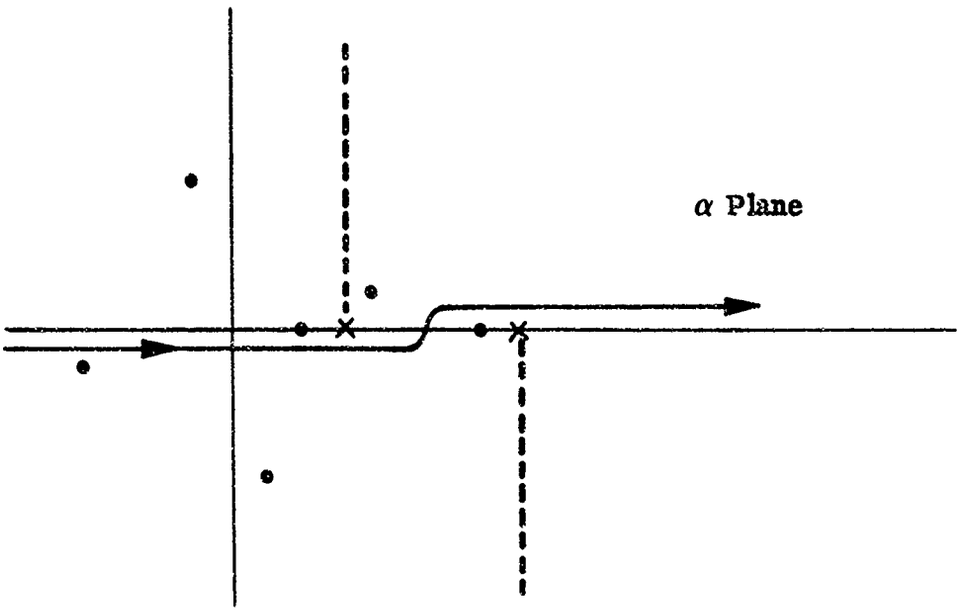

Figure 6. Integration Contour for Γ_{mnrs}

The above contour, Figure 6, is deformed to circulations about poles and branch cut in the appropriate half-planes of analyticity as indicated below, Figure 7, for the upper half-plane.

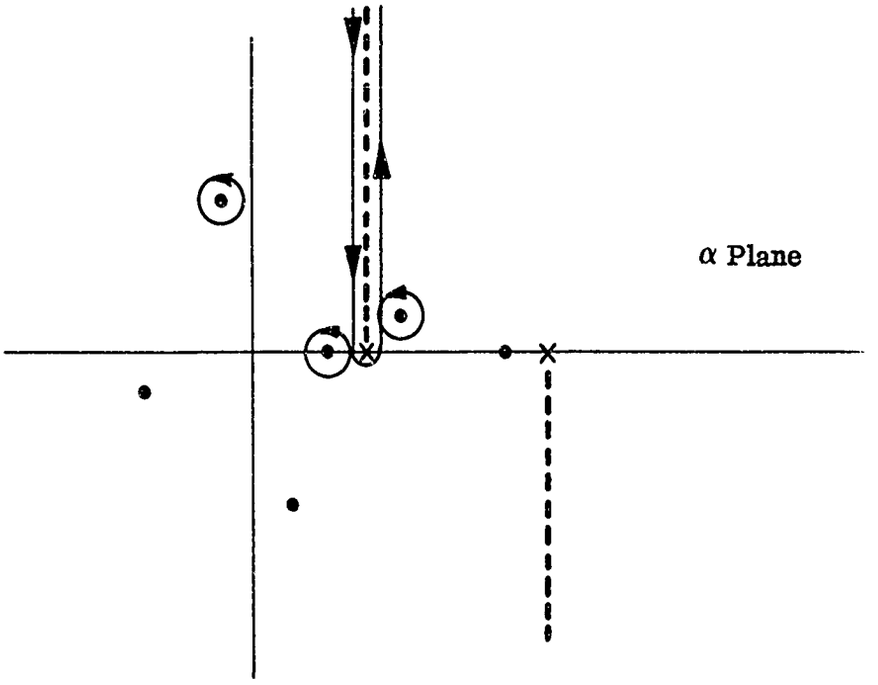

Figure 7. Deformed Integration Contours for Γ_{mnrs}

The function Υ has been analytically continued into the k-plane by giving k a small negative imaginary part; so that, the branch points and the poles are displaced off the real axis as indicated in the previous figures.

The branch-cut integral is given by

$$I(\beta) = \int_0^\infty d\,t \frac{\psi_m(a\,\alpha)\left[B\Lambda(\alpha,\beta) - \Omega(\alpha,\beta)\right]\left(-\frac{2\,i\,\rho_o c^2 (k - M)^2}{\sqrt{k^2 + (M^2-1)\alpha^2 - 2\,kM\,\alpha - \beta^2}}\right)}{(B(\alpha^2+\beta^2)^2 - \rho_p\omega^2)^2 + \left(\frac{\rho_o c^2 (k - \alpha M)^2}{\sqrt{k^2 + (M^2-1)\alpha^2 - 2\,k\,M\alpha - \beta^2}}\right)^2}$$

where $\alpha = A_s^- - i\,t$

So that

$$\Gamma_{mnrs} = \int 2\pi\,i \sum \text{residues}\, d\,\beta + \int_{-\infty}^{\infty} \psi_n(\beta b)\, I(\beta)\, d\,\beta$$

The branch-cut integral is exponentially damped rather oscillatory, so it may be readily performed numerically using Laguerre-Gauss quadrature. The second integral is more difficult, it oscillates with a period $\frac{2\pi}{b}$.

In solving equation (22) maximum values of the indices are polstulated . This is justified, since the index is inversely proportional to some length on the panel. Now there certainly exists, from the experimental

point of view, a smallest length to which a disturbance may be localized. After having solved equation (22) the plate displacement is simply the Fourier transform of (21), thus,

$$W(\vec{r}) = \sum_{m,n} W_{mn} \varphi_m\left(\frac{x}{a}\right) \varphi_n\left(\frac{y}{b}\right) \qquad (23)$$

where φ_m is a beam eigen function.

To find the sound pressure level in the cavity the expression for W from equation (23) is inserted into equation (5b) to give

$$p_1(\vec{r}) = \frac{\omega^2 \rho_c}{a_c b_c} \sum_{m,n} \sum_{r,s} W_{rs} I_{mr} J_{ns} \frac{\cos\frac{m\pi x_c}{a_c} \cos\frac{n\pi y_c}{b_c} \cos k_{mn}(z+d)}{k_{mn} \sin k_{mn} d}$$

where I_{mr} and J_{ns} are given in the appendix B.

Similarly, the radiation may be computed from equation (12).

The force is not a deterministic function as has been implicitly assumed from the outset, but a stochastic variable whose correlation properties are known, either via a model or directly from experimental data. Thus, it would only be meaningful to compute statistical averages of the response based on statistical averages of the force (i.e. cross-correlation). The procedure to be used is an amendment of a procedure due to Rosenblatt (1962), the notation is that of Rosenblatt.

Consider a homogeneous, stationary, random process $X_{\vec{r},\,t}$ (Rosenblatt writes this as $X_{\vec{r},\,t}(\omega)$ to explicitly indicate that it

is a function defined on a sample space) with a cross-correlation defined as

$$R(\vec{r}, t; \vec{r}', t') = \langle X_{\vec{r}, t} X_{\vec{r}', t'} \rangle \tag{24}$$

where $\langle\ \rangle$ is the expectation operator, i.e., R is defined through an ensemble average. Because the process is homogeneous and stationary,

$$R(\vec{r}, t; \vec{r}', t') = R(\vec{r} - \vec{r}', t - t')$$

or

$$R(\vec{r} - \vec{r}', t - t')\, d\vec{r}\, dt = \langle dM(x_{\vec{r}, t})\, dM(X_{\vec{r}', t'}) \rangle$$

where $dM(x_{\vec{r}, t})$ is the Stieljes measure of the process. The procedure may be simply stated as the problem of finding a Fredholm expansion of R and subsequently representing $X_{r, t}$ by such an expansion. Such an expansion is provided by the eigenfunctions and eigenvalues of the integral equation

$$\psi(\vec{r}, t) = \lambda \int_{-\infty}^{\infty} R(\vec{r} - \vec{r}', t - t')\, \psi(\vec{r}', t')\, d\vec{r}'\, dt \tag{25}$$

The spectrum, is of course, continuous. The eigenfunctions are plane waves and the eigenvalues the inverse of the power spectral density as can be seen by applying the Fourier transform. Thus the desired expansion for R is

$$R(\vec{r} - \vec{r}', t - t') = \left(\frac{1}{2\pi}\right)^2 \int_{-\infty}^{\infty} e^{i[\vec{K} \cdot (\vec{r} - \vec{r}') - (t - t')]} \hat{R}(\vec{K}, \omega)\, d\vec{K}\, d\omega$$

Now let

$$Z_{\vec{K}, \omega} = \frac{1}{(2\pi)^2 \sqrt{R(\vec{K}, \omega)}} \int_{-\infty}^{\infty} e^{i(\vec{K} \cdot \vec{r} - \omega t)} dM(X_{\vec{r}, t}) \tag{26}$$

It follows from (24) and (26) that

$$\langle Z_{\vec{K},\omega} Z^{*}_{\vec{K}',\omega} \rangle = \delta(\vec{K} - \vec{K}')\, \delta(\omega - \omega')$$

Since $\langle d M(X_{\vec{r},t})\, d M^{*}(X_{\vec{r}',t'}) \rangle = R(\vec{r} - \vec{r}', t - t')\, d\vec{r}\, dt$

Thus, the $Z_{K,}$ are independent random variables with unit variance and with zero mean if $E X_{\vec{r},t} = 0$. The transform of (26) is,

$$X_{\vec{r},t} = \int_{-\infty}^{\infty} Z_{\vec{K},\omega} \sqrt{R(\vec{K},\omega)}\, e^{-i(\vec{K}\cdot\vec{r} - \omega t)} d\vec{K} d\omega \qquad (27)$$

A simple calculation reveals that (27) satisfies (24).

These results will now be applied to the plate displacement. Thus, the cross-power spectral density (CPSD) of the plate response is given by (asterisk denotes complex conjugate)

$$\langle W(\vec{r})\, W^{*}(\vec{r}') \rangle = \sum_{m,n,r,s} \varphi_m\left(\frac{x}{a}\right)\varphi_n\left(\frac{y}{b}\right)\varphi_r\left(\frac{x'}{a}\right)\varphi_s\left(\frac{y'}{b}\right) \langle W_{mn} W_{rs}^{*} \rangle \qquad (28)$$

Now if the solution to equation (22) is represented as

$$W_{mn} = \sum_{i,j} \gamma_{mnij}\, \Phi_{ij}$$

then

$$\langle W_{mn}\, W^{*}_{rs} \rangle = \sum_{ijkl} \gamma_{mnij}\, \gamma^{*}_{rskl}\, \langle \Phi_{ij}\, \Phi^{*}_{kl} \rangle$$

Further,

$$\langle \Phi_{ij} \Phi^*_{kl} \rangle = \int_{-\infty}^{\infty}\int_{-\infty}^{\infty} d\vec{K}\, d\vec{K}' \; \frac{\psi_i(\alpha a)\,\psi_j(\beta b)\,\psi^*_k(\alpha' a)\,\psi^*_l(\beta' b)}{\Upsilon(\vec{K})\;\Upsilon^*(\vec{K}')} \; \langle f(\vec{K})\, f^*(\vec{K}') \rangle$$

The force F is now identified with $X_{\vec{r},\,t}$ so that

$$\langle \hat{f}(\vec{K})\; \hat{f}^*(\vec{K}') \rangle = \left[\hat{R}(\vec{K}, \omega)\; \hat{R}^*(\vec{K}', \omega) \right]^{1/2} \langle Z_{\vec{K},\omega}\; Z^*_{\vec{K}',\omega} \rangle$$

$$= \left[\hat{R}(\vec{K}, \omega)\; \hat{R}^*(\vec{K}', \omega) \right]^{1/2} \delta(\vec{K} - \vec{K}')$$

In summary then

$$\langle W_{mn}\, W^*_{rs} \rangle = \sum_{i,j,k,l} \gamma_{mnij}\, \gamma^*_{rskl} \int_{-\infty}^{\infty} d\vec{K} \, \frac{\psi_i(\alpha a)\, \psi_j(\beta b)\; |R(\vec{K},\omega)|\, \psi^*_k(\alpha a)\, \psi^*_l(\beta b)}{|\Upsilon(\vec{K})|^2} \tag{29}$$

Analogous to (28), the expression for the CPSD of P_1 can be written in terms of $E\, W_{mn}\, W^*_{rs}$ from (29). The same can also be done for the radiation.

B. One Dimensional Model

To simplify the computations we assume that the transverse plate dimension is very large and that no flexural waves propagate in the transverse direction. With these simplifications equation (22) may be written

$$W_n \cdot \sum_m \Gamma_{nm} W_m = \Phi_n \tag{30}$$

where

$$\Gamma_{nm} = \int_{-\infty}^{\infty} d K \frac{\psi_n^* (K a) \Lambda \left[\varphi_m \left(\frac{x}{a} \right) \right]}{\Upsilon (K)} \tag{31}$$

where

$$\Upsilon (K) = K^4 - \gamma^4 - \frac{i \mu \gamma^4 \left(1 - \frac{K^2 M^2}{k^2} \right)}{\sqrt{k^2 + (M^2 - 1) K^2 - 2 k K M}}$$

and

$$\Phi_n = \int_{-\infty}^{\infty} d K \frac{\psi_n^* (a K) F (K)}{\Upsilon (K)} \tag{32}$$

The circumvention of the branch points in the above expressions will be described shortly.

If G_{mn} denotes the inverse matrix to $\delta_{mn} + \Gamma_{mn}$ then the solution to (30) is

$$W_n = \sum_m G_{nm} \phi_m$$

Now performing the ensemble averages as before gives

$$\langle W_m W_n^* \rangle = \sum_{r,s} G_{mr} \langle \phi_r \phi_s^* \rangle G^*_{rs} \tag{33}$$

but

$$\langle \phi_r \phi_s^* \rangle = \int_{-\infty}^{\infty} dK \frac{\psi_r^* (aK)}{\Upsilon (K)} \int_{-\infty}^{\infty} dK' \frac{\psi_s (aK')}{\Upsilon^* (K')} \langle F (K) F^* (K') \rangle$$

To make the discussion concrete let

$$\langle F (K) F^* (K') \rangle = P (\omega) \delta (K' - (K - \frac{\omega}{U_c}))$$

which corresponds to a spatially uncorrelated pressure field with convection velocity U_c and power spectrum $P (\omega)$.

Thus,

$$\langle \phi_r \phi_s^* \rangle = P (\omega) \int_{-\infty}^{\infty} dK \frac{\psi_r^* (aK) \psi_s (aK - \frac{a\omega}{U_c})}{\Upsilon (K) \Upsilon^* (K - \frac{\omega}{U_c})} \tag{34}$$

The major contribution to the integral for Γ_{mn}, equation (31), comes about when the peak of ψ_n is close to the peaks of $1/\Upsilon (K)$; since ψ_n is a highly oscillatory function (period $= \frac{2\pi}{a}$) with a peak at $\frac{\chi n}{a}$ and decaying with the distance from this point and $\frac{1}{\Upsilon (K)}$ is a non-oscillatory function with peaks whenever K equals the real part of the poles which are roughly located at γ times the four roots of unit and the trapped wave poles near the branch points $\frac{k}{1+M'} \quad \frac{k}{M-1}$. But for the frequencies we are considering (up to 3000 Hz) only the pole near $\frac{k}{1+M}$ lies on the physical sheet. For this frequency range the trapped wave pole is bounded by 0 and .15 and the pole near γ by 0 and .6. Now, the peak of ψ_n^* is given by $\frac{\chi m}{a}$ which is numerically (see Appendix B) .155, .26, .36, .465, .57, .67, . . . and the period is .206. The height of the peaks decays roughly as $\left(\frac{1}{Ka}\right)^3$ is .05 of the first. The function $\frac{1}{\Upsilon (K)}$ also has peaks that decay in the same

manner. Thus, the infinite matrix Γ_{mn} has appreciably non-zero entries only in the upper left-hand corner. Consequently, we need only compute Γ_{mn} for the first 4 or 5 modes, say, and then invert this matrix + I to obtain the upper left square matrix of order 4 or 5 of G_{mn} and thus for higher modes

$$G_{mn} = \delta_{mn}$$

So that

$$\langle W_m W_n^* \rangle = \langle \phi_m \phi_n^* \rangle$$

for other than the first few modes.

The contour for the integral in (34), Figure 8, is similar to one described earlier but the term $\hat{\Gamma}^* (K - \frac{k}{m})$ introduces further poles and branch cuts. The contour and its deformation are shown in the Figures 8 and 9. In Figure 9 only the contours for that part of the integrand which is analytic in the upper half-plane are shown.

$\psi_m (K)$ may be written

$$\psi_m (K) = S_m (K) + T_m (K) e^{-i K a}$$

where

$$S_m (K) = - 4 N_m \frac{i \alpha_m (a K)^3 - \chi_m^3}{(a K)^4 - \chi_m^4}$$

and

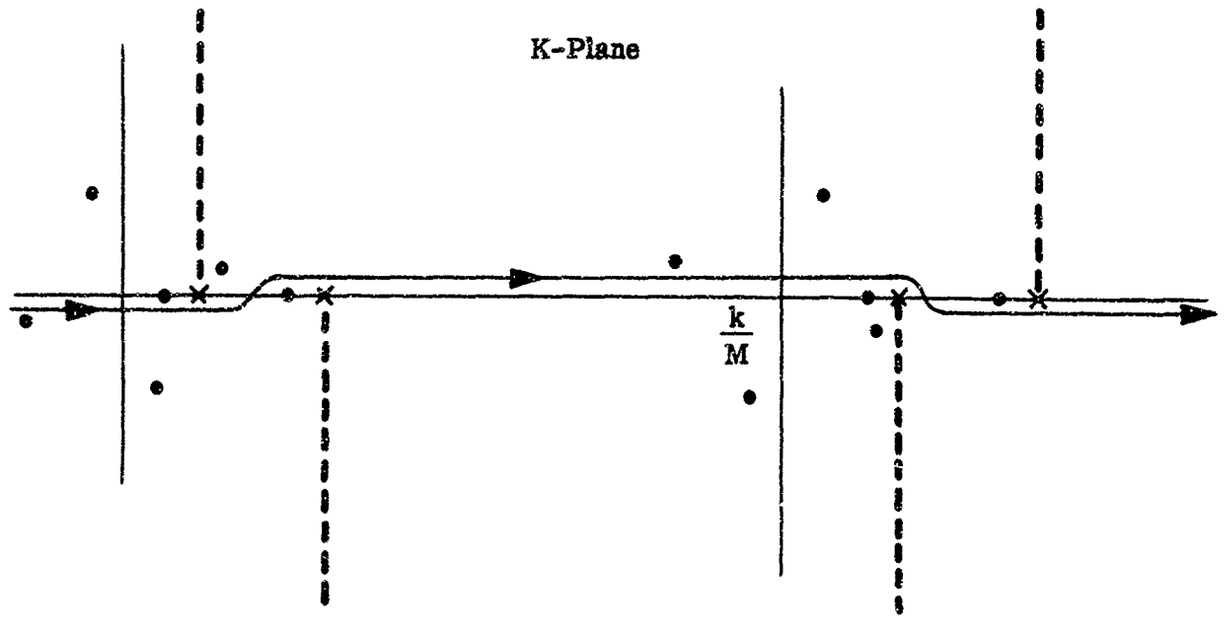

Figure 8. Contour for $\langle \phi_r \ \phi_s^* \rangle$ in Equation (34)

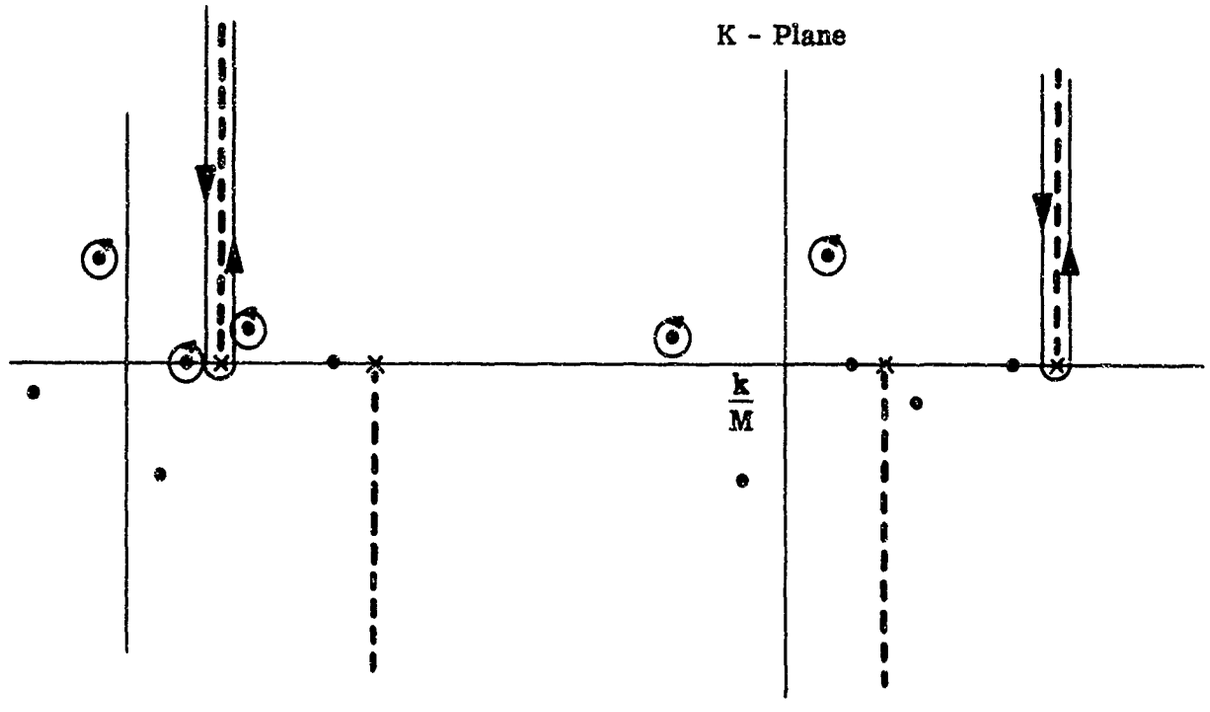

Figure 9. Deformation of contour in Figure 8.

$$\frac{1}{2} T_m(K) = N_m \left[(\chi_m + i\alpha_m a K) \left(\frac{\cos \chi_m}{(aK)^2 - \chi_m^2} - \frac{ch \chi_m}{(aK)^2 + \chi_m^2} \right) \right.$$

$$\left. - (\alpha_m \chi_m - i a K) \left(\frac{\sin \chi_m}{(aK)^2 - \chi_m^2} + \frac{sh \chi_m}{(aK)^2 + \chi_m^2} \right) \right.$$

with α_m and χ_m defined in Appendix B.

Now

$$\psi_m^*(K)\, \psi_n\left(K - \frac{\omega}{v}\right) = L(K) + U(K)$$

where

$$L(K) = S_m^*(K) \left(S_n\left(K - \frac{\omega}{v}\right) + T_n\left(K - \frac{\omega}{v}\right) e^{-i\left(K - \frac{\omega}{v}\right) a} \right)$$

and

$$U(K) = e^{i\frac{a\omega}{v}}\, T_m^*(K) \left(S_n\left(K - \frac{\omega}{v}\right) + T_n\left(K - \frac{\omega}{v}\right) e^{i\left(K - \frac{\omega}{v}\right) a} \right)$$

Thus, we have

$$\langle \phi_m \phi_n^* \rangle = P(\omega) \int_{-\infty}^{\infty} dK\, \frac{L(K) + U(K)}{\Upsilon(K)\, \Upsilon^*\left(K - \frac{\omega}{v}\right)}$$

The above expression is evaluated as a sum of residue contributions plus branch - cut integrals.

$$\frac{1}{P(\omega)} \langle \phi_m \phi_n^* \rangle = 2\pi i \sum_{j=1}^{5} \operatorname{Res} \left\{ \frac{L(z_j)}{\Upsilon(z_j)\, \Upsilon^*\left(z_j - \frac{\omega}{U_c}\right)} \right\} + I_1 + I_2$$

$$+ 2\pi i \sum_{\substack{j=7 \\ j+9}}^{12} \operatorname*{Res}_{z=z_j} \left\{ \frac{L(z)}{\Upsilon(z)\, \Upsilon^*\left(z - \frac{\omega}{U_c}\right)} \right\} + I_3 + I_4$$

where the z_j are identified in the above figure.

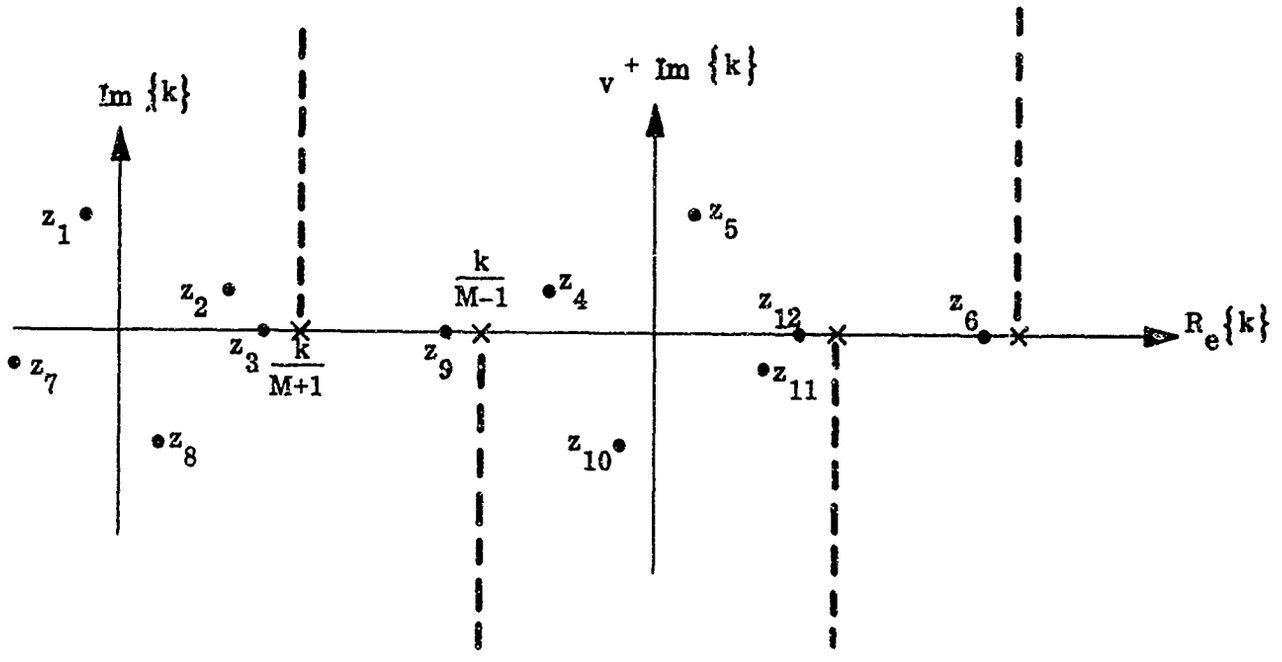

Figure 10. Location of poles and branch cuts

As indicated previously, z_6 and z_9 are not on the physical sheet for the range of frequencies considered (Up to 14000 Hz).

$$I_1 = \int_0^\infty dy \, \frac{U\left(\frac{k}{M+1} + iy\right)}{\Upsilon^*\left(\frac{k}{M+1} - \frac{\omega}{U_c} + iy\right)} \left[\frac{1}{\Upsilon^+\left(\frac{k}{M+1} + iy\right)} - \frac{1}{\Upsilon^-\left(\frac{k}{M+1} + iy\right)} \right]$$

where $\Upsilon^+\left(\frac{k}{M+1} + iy\right)$ is the expression following equation (31) the plus being included only to explicate that it is the positive side of the square root branch cut. $\Upsilon^-\left(\frac{k}{M+1} + iy\right)$ is obtained from Υ^+ by replacing μ by $-\mu$.

$$I_2 = -\int_0^\infty dy \; \frac{U\left(\frac{k}{M-1} + \frac{\omega}{U_c} + iy\right)}{\Upsilon\left(\frac{k}{M-1} + \frac{\omega}{U_c} + iy\right)} \left[\frac{1}{\Upsilon^{+*}\left(\frac{k}{M-1} + iy\right)} - \frac{1}{\Upsilon^{-*}\left(\frac{k}{M-1} + iy\right)} \right]$$

$$I_3 = -\int_0^\infty dy \; \frac{L\left(\frac{k}{M-1} - iy\right)}{\Upsilon^{*}\left(\frac{k}{M-1} - \frac{\omega}{U_c} - iy\right)} \left[\frac{1}{\Upsilon^{+}\left(\frac{k}{M-1} - iy\right)} - \frac{1}{\Upsilon^{-}\left(\frac{k}{M-1} + iy\right)} \right]$$

$$I_4 = \int_0^\infty dy \; \frac{L\left(\frac{k}{M-1} + \frac{\omega}{U_c} - iy\right)}{\Upsilon\left(\frac{k}{M+1} + \frac{\omega}{U_c} - iy\right)} \left[\frac{1}{\Upsilon^{+*}\left(\frac{k}{M+1} - iy\right)} - \frac{1}{\Upsilon^{-*}\left(\frac{k}{M+1} - iy\right)} \right]$$

It is felt, that the effect of the pole at z_3 cancels the contribution of I_1 and similarily the residue at z_{12} cancels the contribution of I_3. Thus only I_2 and I_4 will contribute. Therefore

$$\frac{1}{P(\omega)} \langle \phi_m \quad \phi_n^* \rangle = 2\pi i \sum_{\substack{j=1 \\ j\neq 3}}^{5} \operatorname*{Res}_{z=z_j} \left\{ \frac{U(z)}{\Upsilon(z)\, \Upsilon^*\left(z - \frac{\omega}{U_c}\right)} \right\} + I_2$$

$$+ 2\pi i \sum_{\substack{j=7 \\ j\neq 9}}^{11} \operatorname*{Res}_{z=z_j} \left\{ \frac{L(z)}{\Upsilon(z)\, \Upsilon^*\left(z - \frac{\omega}{U_c}\right)} \right\} + I_4$$

By the same argument which eliminated I_1 and I_3 we may replace I_2 and I_4 by pretending that z_6 and z_9 are on the physical sheet and thus

$$I_2 = -2\pi i \operatorname*{Res}_{z=z_6} \left\{ \frac{U(z)}{\Upsilon(z)\, \Upsilon^*\left(z - \frac{\omega}{U_c}\right)} \right\}$$

and

$$I_4 = -2\pi i \operatorname*{Res}_{z=z_9} \left\{ \frac{L(z)}{\Upsilon(z)\,\Upsilon^*\left(z - \frac{\omega}{U_c}\right)} \right\}$$

To evaluate the residues it is necessary to determine

$$\Upsilon'(z) = 4z^3 + \frac{i\mu\gamma^4 (3 z M^2 k^2 + z^3 M^4 - z^3 M^2 - 3 k M^3 z^2 - k^2 z - k^3 M)}{\sqrt{k^2 + (M^2 - 1) z^2 - 2 k M z}^3}$$

The following relationships among the poles are valid

$$z_4 = \frac{\omega}{U_c} + z_7^* \qquad z_5 = \frac{\omega}{U_c} + z_8^* \qquad z_6 = \frac{\omega}{U_c} + z_9$$

$$z_{10} = \frac{\omega}{U_c} + z_1^* \qquad z_{11} = \frac{\omega}{U_c} + z_2^*$$

$$\lim_{z \to z_4} \left[\frac{z - z_4}{\Upsilon^*\left(z - \frac{\omega}{U_c}\right)} \right] = \lim_{z \to z_7^*} \left[\frac{z - z_7^*}{\Upsilon^*(z)} \right] = \lim_{z \to z_7} \left[\frac{z - z_7}{\Upsilon^*(z^*)} \right]$$

$$\Upsilon^*(z) = z^{*4} - \gamma^4 + \frac{i\mu\gamma^4 \left(1 - \frac{z^{*2} M^2}{k^2}\right)}{\sqrt{k^2 + (M^2 - 1) z^{*2} - 2 k M z^*}}$$

So

$$\Upsilon^*(z^*) = \Upsilon^-(z)$$

Thus

$$\lim_{z \to z_4} \left[\frac{z - z_9}{\Upsilon^* \left(z - \frac{\omega}{U_c}\right)} \right] = \Upsilon^{-1}(z_7)$$

Similarly

$$\lim_{z \to z_5} \left[\frac{z - z_5}{\Upsilon^* \left(z - \frac{\omega}{U_c}\right)} \right] = \Upsilon^{-1}(z_8)$$

$$\lim_{z \to z_y} \left[\frac{z - z_6}{\Upsilon^* \left(z - \frac{\omega}{U_c}\right)} \right] = \Upsilon^{-1}(z_9)$$

$$\lim_{z \to z_{10}} \left[\frac{z - z_{10}}{\Upsilon^* \left(z - \frac{\omega}{U_c}\right)} \right] = \Upsilon^{-1}(z_1)$$

$$\lim_{z \to z_{11}} \left[\frac{z - z_4}{\Upsilon^* \left(z - \frac{\omega}{U_c}\right)} \right] = \Upsilon^{-1}(z_2)$$

$$\frac{1}{2\pi i P(\omega)} \langle \phi_m \phi_n^* \rangle = \frac{U(z_1)}{\Upsilon'(z_1)\,\Upsilon^*\left(z_1 - \frac{\omega}{U_c}\right)} + \frac{U(z_2)}{\Upsilon'(z_2)\,\Upsilon^*\left(z_2 - \frac{\omega}{U_c}\right)}$$

$$+ \frac{U\left(\frac{\omega}{U_c} + z_7^*\right)}{\Upsilon\left(\frac{\omega}{U_c} + z_7^*\right)\Upsilon^{-1}(z_7)} + \frac{U\left(\frac{\omega}{U_c} + z_8^*\right)}{+\Upsilon\left(\frac{\omega}{V} + z_8^*\right)\Upsilon^{-1}(z_8)}$$

$$- \frac{U\left(\frac{\omega}{U_c} + z_9\right)}{\Upsilon\left(\frac{\omega}{U_c} + z_9\right)\Upsilon^{-1}(z_9)}$$

$$+ \frac{L(z_7)}{\Upsilon'(z_7)\,\Upsilon^*\left(z_7 - \frac{\omega}{V}\right)} + \frac{L(z_8)}{\Upsilon'(z_8)\,\Upsilon^*\left(z_8 - \frac{\omega}{U_c}\right)}$$

$$+ \frac{L\left(\frac{\omega}{U_c} + z_1^*\right)}{\Upsilon\left(\frac{\omega}{U_c} + z_1^*\right) \Upsilon^{-1}(z_1)} + \frac{L\left(\frac{\omega}{U_c} + z_2^*\right)}{\Upsilon\left(\frac{\omega}{U_c} + z_2^*\right) \Upsilon^{-1}(z_2)}$$

$$- \frac{L(z_9)}{\Upsilon'(z_9)\,\Upsilon^*\left(z_9 - \frac{\omega}{U_c}\right)}$$

In a similar, though simpler fashion, we may evaluate the integral in equation (32).

$$\Lambda\left[\phi_m\left(\frac{x}{a}\right)\right] = A_m(K) + B_m(K)\, e^{-iKa}$$

where

$$A_m(K) = -\frac{2N_m}{a}\left(\frac{\chi_m}{a}\right)^2 \left[\chi_m - \frac{\cos\chi_m - \mathrm{ch}\,\chi_m}{\sin\chi_m + \mathrm{sh}\,\chi_m}\, iKa\right]$$

and

$$B_m(K) = -\frac{2N_m}{a}\left(\frac{\chi_m}{a}\right)^2 \left[\frac{\chi_m(\cos\chi_m\,\mathrm{sh}\,\chi_m + \sin\chi_m\,\mathrm{ch}\,\chi_m) - iKa\sin\chi_m\,\mathrm{sh}\,\chi_m}{\sin\chi_m + \mathrm{sh}\,\chi_m}\right]$$

Thus $\psi_n^* \Lambda\left[\phi_m\right]$ may be decomposed into factors analytic in upper and lower half-planes, respectively. Denoting these terms by G^+ and G^- we have,

$$\Gamma_{mn} = \int_{-\infty}^{\infty} \frac{G^+(K) + G^-(K)}{\Upsilon(K)}\, dK$$

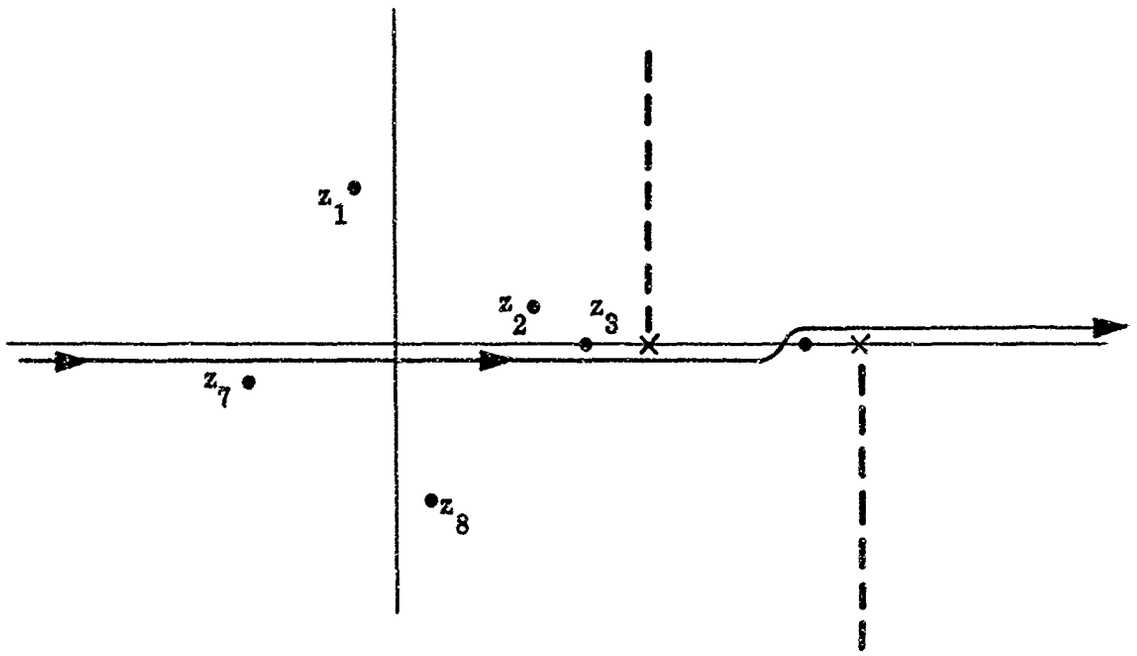

Figure 11. Contour for Γ_{mn} equation (31)

where

$$G^{+}(K) = A_m(K)\left(S_n^*(K) + T_n^*(K)\, e^{iKa}\right)$$

and

$$G^{-}(K) = B_m(K)\left(T_n^*(K) + S_n^*(K)\, e^{-iKa}\right)$$

The contour of integration is indicated above .

The contour is deformed in the appropriate half-planes and branch cuts are replaced by poles ad discussed previously. Thus,

$$\frac{1}{2\pi i}\,\Gamma_{mn} = \operatorname*{Res}_{z=z_1}\left\{\frac{G^{+}(z)}{\Upsilon(z)}\right\} + \operatorname*{Res}_{z=z_1}\left\{\frac{G^{+}(z)}{\Upsilon(z)}\right\}$$

$$- \operatorname*{Res}_{z=z_7}\left\{\frac{G^{-}(z)}{\Upsilon(z)}\right\} - \operatorname*{Res}_{z=z_8}\left\{\frac{G^{-}(z)}{\Upsilon(z)}\right\}$$

$$+ \operatorname*{Rex}_{z=z_9}\left\{\frac{G^{-}(z)}{\Upsilon(z)}\right\}$$

We now invert the matrix $\delta_{mn} + \Gamma_{mn}$. Let us denote this inverse by G_{ij}. Then

$$\langle W_m W_n^* \rangle = G_{mp} \langle F_p F_g^* \rangle \tilde{G}_{gn}$$

where the tilde denotes Hermition conjugate and sum of p and q is implied. The final step, then, becomes the diagonalization of the CPSD matrix $\langle W_m W_u^* \rangle$ thus giving the PSD for the actual degrees of freedom of the system.

C. Acoustic Power, Power Radiated

In computing the power radiated, we make use of the unitary matrix U_{ij} which diagonalized the CPSD matrix. The average power radiated, to the far field, P, is given by

$$P \sim \langle \mathrm{Im} \left\{ \psi^* \frac{\partial \psi}{\partial r} \right\} \rangle$$

By using the asymptotic form of the Hankel function, the asymptotic form of ψ may be computed. This form is

$$\psi(r, \theta) \underset{r \to \infty}{\longrightarrow} \frac{A(\theta)\, e^{i \frac{k r \left(\sqrt{1 - M^2 \sin^2\theta} + M \cos\theta \right)}{M^2 - 1}}}{\sqrt{2\pi i\, k\, r}\, \sqrt{1 - M^2 \sin^2\theta}}$$

where

$$A(\theta) = \int_0^a dx'\, e^{i \frac{k x'}{M^2 - 1} \left(\frac{\cos\theta}{\sqrt{1 - M^2 \sin^2\theta}} - M \right)} W(x')$$

The acoustic velocity in the radial direction u_r is given by

$$u_r = \frac{d\psi}{dr}(r, \theta)$$

$$= \frac{i k\left(\sqrt{1 - M^2 \sin^2 \theta} + M \cos\theta\right)}{M^2 - 1} \psi (r, \theta)$$

The pressure, p, a microphone in the far-field would measure is given by

$$\frac{1}{\rho c} P = i k \psi - M \frac{\partial \psi}{\partial x}$$

$$= i k \psi - \frac{i k M^2}{M^2 - 1} \psi$$

$$= -\frac{i k \psi (r,\theta)}{M^2 - 1}$$

The average radiated intensity is given by the expectation value

$$I = \frac{1}{2} \text{Re} \langle p\, u^* \rangle$$

$$= -\frac{i k \rho c}{M^2 - 1} \frac{i k\left(\sqrt{1 - M^2 \sin^2\theta} + M \cos\theta\right)}{M^2 - 1} \frac{1}{2} \text{Re} \langle \psi \psi^* \rangle$$

$$= \frac{\rho c k^2 \left(\sqrt{1 - M^2 \sin^2 \theta} + M \cos\theta\right)}{2 (M^2 - 1)^2} \text{Re} \langle \psi \psi^* \rangle$$

Now,

$$\langle \psi\, \psi^* \rangle = \frac{1}{(2 \pi k r) \sqrt{1 - M^2 \sin^2\theta}} \langle A (\theta)\ A^* (\theta) \rangle$$

where

$$\langle A (\theta) A^* (\theta) \rangle = \int_0^a dx \int_0^a dx'\, e^{i \frac{k (\mathbf{x}' \cdot \mathbf{x})}{M^2 - 1} \left(\frac{\cos\theta}{\sqrt{1 - M^2 \sin^2\theta}} - M\right)}$$

$$\langle W (x') W^* (x) \rangle$$

and where

$$\langle W(x')\, W^*(x)\rangle = \sum_m \sum_n \langle W_m\, W_n^*\rangle\ \varphi_m(x')\ \varphi_n(x)$$

Let U_{ij} denote the unitary matrix which diagonalizes $\langle W_m\, W_n^*\rangle$, i.e., the transformation to the actual degrees of freedom. Further, let λ_m denote the power in the m^{th} degree of freedom, then we have

$$\langle W(x')\, W^*(x)\rangle = \sum_{i,j,m,n} \varphi_i(x')\ U_{mi}\ \lambda_i\ \delta_{ij}\ U^*_{nj}\ \varphi_n(x)$$

The integrals have already been encountered, they are simply the finite Fourier transform of the $\varphi_m(x)$ so that,

$$\langle A(\theta)\, A^*(\theta)\rangle = \sum_{i,j,m,n} \psi_i(z)\ U_{mi}\ \lambda_i\ \delta_{ij}\ U^*_{nj}\ \psi_j(-z)$$

where

$$z = \frac{ik\,\dfrac{\cos\theta}{\sqrt{1 - M^2\sin^2\theta}} - M}{M^2 - 1}$$

References

Corcos, G.M. (1963) — Resolution of Pressure in Turbulence. J. Acoustic Soc. America Vol. 35, N2.

Crighton, D.G. (1970) — Radiation from Turbulence Near a Composite Flexible Boundary. PRDC. Rog. Soc. London A314, 153-173.

Crighton, D.G. and Ffowcs-Williams, J.E. (1969) — Real Space-Time Green's Functions Applied to Plate Vibration Induced by Turbulent Flow. J. Fluid. Mech. Vol. 38 Part 2, PP 305-313.

Dolgove, I.I. (1969) — Sound Radiation from a Boundary Layer Soviet Physics Acoustics Vol. 15, No. 1, July-Sept. 1969.

Dowell, E. H. (1969) — Transmission of Noise from a Turbulent Boundary Layer Through a Flexible Plate Into a Closed Cavity. J. Acoustic Soc. America Vo. 46.

Dżygadlo, Z. (1967) — Forced Vibration of Plate of Finite Length in Plane Supersonic Flow. Proc. Vibration Problem, Warsaw, 1,8.

Fahy, A. J. Pretlove (1967) — Acoustic Forces on a Flexible Panel Which is Part of Duct Carrying Airflow. J. Sound & Vibration, Vo. 5.

Feit, D. (1966) — Pressure Radiated by a Point-Excited Elastic Plate. J. Acoustic Soc. Vol. 40, No. 6, Pp 1489-1494.

Ffowcs-Williams, J.E. (1966) — The Influence of Simple Supports on the Radiation From Turbulent Flow Near a Plane Compliant Surface. J. Fluid Mech. Vol. 26, Part 4, PP 641-649.

References - Continued

Lapin, A.D. (1967) — Radiation of Sound by a Vibrating Non-Uniform Wall. Soviet Physics - Acoustics Vol. 13, No. 1, July-Sept. Pp 55-58.

Lyamshev, L.M. (1968) — On the Sound Radiation Theory From Turbulent Flow Near an Elastic Inhomogeneous Plate. The 6th Internation Congress of Acoustics, Tokyo.

Maestrello, L. (1969) — Radiation From and Panel Response to Supersonic Turbulent Boundary Layer. J. Sound Vibration (10) 2.

Magnus, W. and Oberhettinger, F. (1961) — Formulas and Theorems for the Special Functions of Mathematical Physics. Chelsea.

Morse, P. and Feshback, H. (1953) — Methods of Theoretical Physics Chap. 11, McGraw Hill, New York.

Pol'tov, V.A. and Pupyzev, V.A. (1967) — Vibration and Sound Radiation of a Plate Under Random Loading. Soviet-Physic Acoustics Vol. 13, No. 2, Oct-Dec. Pp 210-214.

Rosenblatt, M. (1962) — Random Processes. Chap. VIII. Oxford University Press, New York.

Strawderman, W.A. (1967) — The Acoustic Field in a Closed Space Behind a Rectangular Simply Supported Plate Excited by Boundary Layer Turbulence. USL Report No. 827.

White, P.H. Cottis, M.G. (1968) — Acoustic Radiation From a Plate - Rib System Excited by Boundary Layer Turbulence. Measurement Analysis Corporation 702-06.

APPENDIX A

If we make the following changes in variables

$$\xi = \sqrt{(M^2 - 1)}\,\alpha - \kappa M$$

$$\kappa = \frac{k}{\sqrt{M^2 - 1}}$$

$$u = \frac{x - x'}{\sqrt{M^2 - 1}}$$

then expression for the Green's function in equation (9) becomes

$$G(x, y, z \mid x', y', 0) = \frac{e^{i\kappa M u}}{\sqrt{M^2 - 1}} \int_{-\infty}^{\infty}\int_{-\infty}^{\infty} d\xi d\beta \, \frac{e^{i\left[\xi u + \beta(y-y') + z\sqrt{\xi^2 - (\kappa^2 + \beta^2)}\right]}}{\sqrt{\xi^2 - (\kappa^2 + \beta^2)}}$$

$$= \frac{e^{i\kappa M u}}{\sqrt{M^2 - 1}} \int_{-\infty}^{\infty} d\xi \, e^{i\xi u} \int_{-\infty}^{\infty} \frac{d\beta e^{i\left[\beta(y-y') + z\sqrt{(\xi^2 - \kappa^2) - \beta^2}\right.}}{(\xi^2 - \kappa^2) - \beta^2}$$

(see M + F Vol. I Page 823)

$$= \frac{\pi e^{i\kappa M u}}{\sqrt{M^2 - 1}} \int_{-\infty}^{\infty} d\xi \, e^{i\xi u} \, H_o^{(1)}\left(R\sqrt{\xi^2 - \kappa^2}\right)$$

$$R^2 = (y - y')^2 + z^2$$

The contour of integration for the above integral is shown below

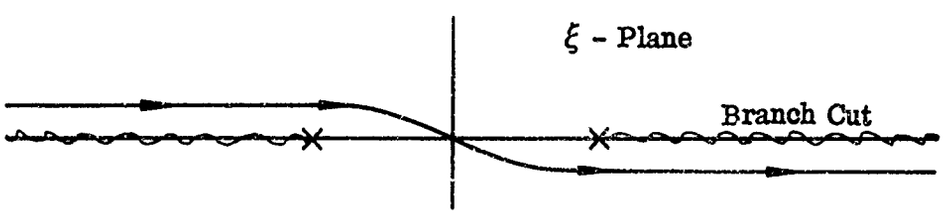

Define

$$I(u) = \int_{-\infty}^{\infty} d\xi \, e^{i\xi u} \, H_0^{(1)} \left(R\sqrt{\xi^2 - \kappa^2}\right)$$

By considering the asymptotic form of the Hankel function, the above integral is seen to be convergent in the upper half-plane for values of u and R such that

$$u > R$$

that is, the region inside the Mach cone

The contour may be deformed to be a contour along the branch cut as shown below

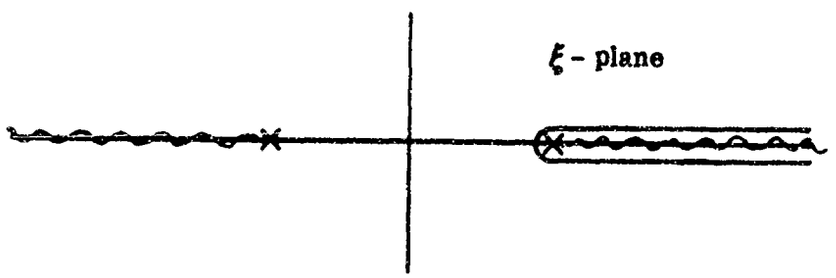

Thus

$$I(u) = \left[\int_{\kappa}^{\infty} + \int_{-\infty}^{\kappa} \right] e^{i\xi u} \, H_0^{(1)} \left(R\sqrt{\xi^2 - \kappa^2}\right) d\xi$$

below cut above cut

$$= \int_{\kappa}^{\infty} e^{i\xi u} \, H_0^{(2)} \left(R\sqrt{\xi^2 - \kappa^2}\right) - \int_{\kappa}^{\infty} e^{i\xi u} \, H_0^{(1)} \left(R\sqrt{\xi^2 - \kappa^2}\right) d\xi$$

$$= -2 \int_{\kappa}^{\infty} e^{i\xi u} \, J_0 \left(R\sqrt{\xi^2 - \kappa^2}\right) d\xi$$

We thus get (see Magnus & Oberhettinger p. 179)

$$I(u) = 2i \frac{e^{i\kappa\sqrt{u^2 - R^2}}}{\sqrt{u^2 - R^2}}$$

so that

$$G(\vec{r} \mid \vec{r}') = \frac{2\pi i}{\sqrt{M^2 - 1}} \frac{e^{i\kappa(Mu + \sqrt{u^2 - R^2})}}{\sqrt{u^2 - R^2}}$$

$$= \frac{2\pi i}{\sqrt{M^2 - 1}} \frac{e^{i\kappa M R(\cos\theta + \sin\theta)}}{R \sin\theta}$$

APPENDIX B

$$I_{mr} = \int_0^a \cos \frac{m\pi x_c}{a_c} \; \varphi_r\left(\frac{x}{a}\right) dx$$

$$x_c = x + \frac{a_c - a}{2}$$

$$\varphi_r\left(\frac{x}{a}\right) = \sin \frac{\kappa_r x}{a} - \mathrm{sh} \frac{\kappa_r x}{a} + \alpha_r \left(\cos \frac{\kappa_r x}{a} - \mathrm{ch} \frac{\kappa_r x}{a}\right)$$

$$\frac{1}{N_r} I_{mr} = \frac{1}{\left(\frac{\alpha_r}{a} - \frac{m\pi}{a_c}\right)} \Bigg\{ \alpha_r \left(\sin\left[\left(\frac{\kappa_r}{a} - \frac{m\pi}{a_c}\right) a - \frac{m\pi}{a_c}\left(\frac{a_c - a}{2}\right)\right] + \sin\left[\frac{m\pi}{a_c}\left(\frac{a_c - a}{2}\right)\right] \right)$$

$$+ \cos\left[\frac{m\pi}{a_c}\left(\frac{a_c - a}{2}\right)\right] - \cos\left[\left(\frac{\kappa_r}{a} - \frac{m\pi}{a_c}\right) a - \frac{m\pi}{a_c}\left(\frac{a_c - a}{2}\right)\right] \Bigg\}$$

$$+ \frac{1}{2\left(\frac{\kappa_r}{a} + \frac{m\pi}{a_c}\right)} \Bigg\{ \cos\left[\frac{m\pi}{a_c}\left(\frac{a_c - a}{2}\right)\right] - \cos\left[\left(\frac{\kappa_r}{a} + \frac{m\pi}{a_c}\right) a + \frac{m\pi}{a_c}\left(\frac{a_c - a}{2}\right)\right]$$

$$+ \alpha_r \left(\sin\left[\left(\frac{\kappa_r}{a} + \frac{m\pi}{a_c}\right) a + \frac{m\pi}{a_c}\left(\frac{a_c - a}{2}\right)\right] - \sin\left[\frac{m\pi}{a_c}\left(\frac{a_c - a}{2}\right)\right] \right) \Bigg\}$$

$$+ \frac{\frac{\alpha_r}{a}}{\left(\frac{\kappa_r}{a}\right)^2 + \left(\frac{m\pi}{a_c}\right)^2} \Bigg\{ \cos\left[\frac{m\pi}{a_c}\left(\frac{a_c - a}{2}\right)\right] - \cos\left[\frac{m\pi}{a_c}\left(\frac{a + a_c}{2}\right)\right] \left(\mathrm{ch}\ \kappa_r + \alpha_r \mathrm{sh}\ \kappa_r\right) \Bigg\}$$

$$+ \frac{\frac{m\pi}{a_c}}{\left(\frac{\kappa_r}{a}\right)^2 + \left(\frac{m\pi}{a_c}\right)^2} \Bigg\{ \alpha_r \sin\left[\frac{m\pi}{a_c}\left(\frac{a_c - a}{2}\right)\right] - \mathrm{sh}\left[\frac{m\pi}{a_c}\left(\frac{a + a_c}{2}\right)\right] \left(\mathrm{sh}\ \kappa_r + \alpha_r \mathrm{ch}\ \kappa_r\right) \Bigg\}$$

where

$$\alpha_r = \frac{\cos \kappa_r - \text{ch}\, \kappa_r}{\sin \kappa_r + \text{sh}\, \kappa_r}$$

and the normalization N_r is given by (Dzygadlo 1967) $N_r^{-2} = \frac{1}{4\kappa_r}$

$$(\text{sh}\, 2\kappa_r - \sin 2\kappa_r) + \frac{1}{\kappa_r} (\text{sh}\, \kappa_r \cos \kappa_r - \sin \kappa_r\, \text{ch}\, \kappa_r) + \frac{\alpha_r}{2\kappa_r}$$

$$(\text{ch}\, 2\kappa_r - \cos 2\kappa_r - 4 \sin \kappa_r\, \text{sh}\, \kappa_r) + \alpha_r^2 \left[1 + \frac{1}{4} (\sin 2\kappa_r + \text{sh}\, 2\kappa_r) \right.$$

$$\left. - \frac{1}{\kappa_r} (\sin \kappa_r\, \text{ch}\, \kappa_r + \text{sh}\, \kappa_r \cos \kappa_r) \right]$$

and the eigenvalues κ_r are the roots of the equation

$$\cos\ \kappa_r \cos \text{h}\ \kappa_r = 1$$

and are approximately given by

$$\kappa_1 = 4.730 \quad \kappa_2 = 7.853 \quad \kappa_r = \frac{\pi}{2}(2n + 1)$$

J_{ns} is the same as I_{ns} with a and a_c replaced by b and b_c, respectively.

APPENDIX C

$$\Lambda[w] = \oint d\vec{r}_s \left[\frac{\partial^3 w}{\partial_n^3} - i(\vec{K} \cdot \vec{n}) \frac{\partial^2 w}{\partial_n^2} \right] e^{-i\vec{K}\cdot\vec{r}}$$

Now

$$\Lambda\left[\varphi_m\left(\frac{x}{a}\right)\varphi_n\left(\frac{y}{b}\right)\right] = Q(m, n, \alpha, \beta, a, b)$$

$$- Q(n, m, \beta, \alpha, b, a)$$

where φ is defined in Appendix A and

$$Q(m, n, \alpha, \beta, a, b) = 2\left(\frac{\kappa_n}{b}\right)^2 \left[\frac{\kappa_n}{b} - i\alpha_n\beta + e^{-i\beta b} \cdot \left(\frac{\kappa_n}{b} \operatorname{ch} \kappa_n + i\beta \frac{\operatorname{sh}^2 \kappa_n}{\sin \kappa_n - \operatorname{sh} \kappa_n}\right)\right] \int_0^a dx e^{-i\alpha x} \varphi_m\left(\frac{x}{a}\right)$$

The integral may be found by appropriately combining the following four integrals

$$\int_0^a \sin \kappa_n \frac{x}{a} e^{i\alpha x} dx = \frac{1}{2i}\left[\frac{e^{i(\kappa_n + \alpha a)}}{i\left(\frac{\kappa_n}{a} + \alpha\right)} - \frac{e^{-i(\kappa_n - \alpha a)} - 1}{i\left(\alpha - \frac{\kappa_n}{a}\right)}\right]$$

$$= \frac{a}{2}\left[\frac{e^{i(\alpha a - \kappa_n)} - 1}{\alpha a - \kappa_n} - \frac{e^{i(\alpha a + \kappa_n)} - 1}{\alpha a + \kappa_n}\right]$$

$$\int_0^a \cos\kappa_n \frac{x}{a} e^{i\alpha x} dx = \frac{a}{2i}\left[\frac{e^{i(\alpha a + \kappa_n)}-1}{\alpha a + \kappa_n} + \frac{e^{i(\alpha a - \kappa_n)}-1}{\alpha a - \kappa_n}\right]$$

$$\int_0^a \text{sh}\ \kappa_n \frac{x}{a} e^{i\alpha x} = \frac{ai}{2}\left[+\frac{e^{i(\alpha a + i\kappa_n)}-1}{\alpha a + i\kappa_n} - \frac{e^{i(\alpha a - i\kappa_n)}-1}{\alpha a - i\kappa_n}\right]$$

$$\int_0^a \text{ch}\ \kappa_n \frac{x}{a} e^{i\alpha x} = \frac{a}{2i}\left[\frac{e^{i(\alpha a + i\kappa_n)}-1}{\alpha a + i\kappa_n} + \frac{e^{i(\alpha a - i\kappa_n)}-1}{\alpha a - i\kappa_n}\right]$$

and where α_n is given in Appendix B.

APPENDIX D

$$\Omega\,[w] = \frac{\omega^2 \rho_c}{4\pi} \int_{\text{plate}} d\vec{r}_s \;\; \hat{g}\,(\vec{k}\,|\,\vec{r}_s)\;\; W\,(\vec{r}_s)$$

$$\Omega\,\left[\varphi_r\left(\frac{x}{a}\right)\varphi_s\left(\frac{y}{b}\right)\right] = \omega^2 \rho_c \sum_{\substack{m=o \\ n=o}}^{\infty} \varepsilon_m \varepsilon_n \frac{f_m(\alpha a_c)\, f_n(\beta b_c)\, I_{mr}\, I_{ns}}{k_{mn} \sin k_{mn} d}$$

where

$$f_m(x) = \frac{x\, e^{i(m\pi - x)}}{x^2 - (m\pi)^2}$$

and I_{mr} is given in appendix B.

End

Date Filed

7-20-70